Aerospace Science and Technology 112 (2021) 106635

Contents lists available at ScienceDirect

Aerospace Science and Technology

www.elsevier.com/locate/aescte

Geometrically nonlinear flexural analysis of multilayered composite plate using polynomial and non-polynomial shear deformation theories

Surendra Verma, Babu Ranjan Thakur *, B.N. Singh, D.K. Maiti

Department of Aerospace Engineering, IIT Kharagpur, West Bengal, 721302, India

ARTICLE INFO

Article history:
Received 18 November 2020
Received in revised form 16 February 2021
Accepted 2 March 2021
Available online 17 March 2021
Communicated by Jang-Kyo Kim

Keywords:
Green-Lagrange nonlinearity
Higher-order shear deformation theory (HSDT)
Finite element method

ABSTRACT

In this paper, the geometrically nonlinear bending analysis of multilayered composite plates is carried out through a rigorous comparative study employing Green-Lagrange and von Kármán nonlinearity. The responses are analyzed for various transverse loads and boundary conditions, and emphasized the impending structural condition, which requires the consideration of full geometric nonlinearity. The study is conducted using a C^0 finite element plate model using third-order and non-polynomial shear deformation theories (TSDT and NPSDT). The principle of virtual work is utilized to formulate the weak-form of governing equations, and discretized using nine-noded Lagrange elements with seven degrees-of-freedom per node. The performance of the present model has been validated by comparing present results with those available in the literature and obtained ANSYS results. The results reveal that the consideration of Green-Lagrange nonlinearity is essential for plates with all sides subjected to movable simply supported boundary conditions or with one free edge. The present study also provides a clear idea about the utilization of TSDT and NPSDT for the anti-symmetric and symmetric cross-ply plate, respectively, to get more accurate solution. Further, the effect of penalty for various theories and problems is also highlighted, and its prominent impact is asserted for some cases.

1. Introduction

The multilayered composite structures such as laminated and sandwich plates are being widely used in the engineering nowadays, and by virtue of their application, they often undergo large deflection of the order of their thickness. The range of their applications lies in aerospace, automobile, defense, railways, shipbuilding, biomedical, polymeric electronic, and other fields. In other words, these multilayered composite material has almost covered every engineering sector ranging from the deep ocean to high in the sky. The reason for this wide application could be attributed to the high stiffness-to-weight ratio, high strength-to-weight ratio, which are accommodated by the composite material through the optimized ply-orientation and thickness variation of plies. Further, the transverse loads are often prominent in these areas of application, making it necessary to consider the shear deformation and the transverse direction characteristic behavior. The composite plate exhibits more transverse shear effects than the isotropic plate due to their low transverse shear moduli relative to the in-plane Young's moduli [1]. Hence, for a reliable prediction of flexural characteristic of multilayered composite plates, shear deformation need to be considered in the modeling.

Therefore, to facilitate the design and analysis process of the multilayered composite plate, different laminated plate theories have been proposed. First in such is the classical laminated plate theory (CLPT), which relies on the assumption of transverse normality and neglects the transverse shear deformation [2]. Following that, first-order shear deformation theory (FSDT) has been proposed, which relaxes the transverse normality condition and accounts for constant transverse shear deformation. However, this leads to a non-zero traction condition at the top and bottom surfaces of the plate [3]. Later, higher-order shear deformation theories (HSDTs) are developed, which ensure traction free boundary condition at the top and bottom surfaces along with parabolic variation of transverse stresses and yield accurate structural analysis [4].

For multilayered composite plates, HSDTs with five field variables are most popular due to the following properties: simple implementation, cheaper computation, and reasonable accuracy compared to other HSDTs with more than five field variables [4]. These higher-order

* Corresponding author.
E-mail addresses: surendraverma2501@gmail.com (S. Verma), brtjsk@iitkgp.ac.in (B.R. Thakur), bnsingh@aero.iitkgp.ac.in (B.N. Singh), dkmaiti@aero.iitkgp.ac.in (D.K. Maiti).

https://doi.org/10.1016/j.ast.2021.106635
1270-9638/

shear deformation theories (HSDTs) with five field variables either consider displacement fields of higher-order terms from Taylor's series expansion, called polynomial shear deformation theories (PSDTs), or consider non-polynomial function in the displacement field, called non-polynomial shear deformation theory (NPSDT). Among PSDTs, Reddy's third-order shear deformation (TSDT) is well noted for its accuracy and is well diffused among the researchers. While the NPSDTs with non-polynomial function are further classified as trigonometric, algebraic, hyperbolic, exponential, logarithmic, and mixed shear deformation theories. Moreover, the list of NPSDTs is huge [3,4]. Recently, NPSDTs have been used for the static analysis of (advanced) composite plate by various researchers [1,2,5–14]. Among the aforementioned NPSDTs, the accuracy of inverse hyperbolic shear deformation theory (IHSDT), developed by Grover et al. [5], is also well noticed in the literature [1,2,5,6,15]. However, as per authors' knowledge, the various aspects of bending analysis using NPSDTs (IHSDT in the present study) have not been adequately addressed in many ways, like anti-symmetric cross-ply, penalty parameter, etc. Hence, there is an essential need to rectify these discrepancies in the available literature for NPSDT.

Further, the laminated plates, often used as thin plates, exhibit nonlinear behavior under large load amplitude. This nonlinearity is mainly originated due to large displacement, because of the closeness of yield and fracture criteria in the characteristic of laminated composite material. In many instances, the assumption of linearity leads to a reasonable idealization of the system behavior. Moreover, a linear solution is obtained with considerable ease and lesser computation than a nonlinear solution. However, in some cases, this may result in an unrealistic approximation of the response. Over the last decades, the large deformation analysis of the multilayered composite plates has been the subject of interest of many investigators using analytical [16] or numerical [17–21] methods. Among different numerical methods, the finite element method has been the most popular and practical numerical tool for analyzing composite structures.

In general, the finite element method is often based on the displacement approach, which utilizes C^0 continuous Lagrange and C^1 continuous Hermite approximations. However, the C^0 finite element formulation is more prevalent due to ease in the implementation. Furthermore, very few finite element packages provide support for the Hermite element. For instance, among various open-source FE packages, i.e., code_Aster, GetFEM++, Deal II, Range, Elmerfem, MOOSE, libMesh, FEniCS, FEA Tool Multiphysics, Fired ake, COMSOL(R), only GetFEM++ and FEA Tool Multiphysics support Hermite element. Moreover, to utilize C^0 finite element formulation in conjunction with HSDTs, penalty constraints need to be considered to reduce the C^1 continuity of HSDTs. For instance, the C^0 finite element approach has been considered by several investigators [7,8,22–25]. However, most of aforementioned references have not considered the penalty constraints [7,8,23,25]. Whereas, those who have considered have not illustrated the effect of different penalty constraints [22,24]. Moreover, among these, only a few [7,23,25] have focused on nonlinear bending analysis using C^0 FEM.

In the context of nonlinear bending analysis of laminated plate, extensive studies have been carried out by various investigators. However, most of studies are limited to von Kármán nonlinearity [26–28] utilizing different modeling technique, i.e., CLPT [29–31], FSDT [32–37], simplified TSDT [38–40], PSDTs [18,19,41–46], higher-order shear and normal deformation theory (HSNDT) [47], Layerwise theory [48,49] and NPSDTs [7,23,50–52]. On the other hand, very few studies have been conducted incorporating Green-Lagrange nonlinearity [15,53] using FSDT [54,55], PSDTs [56], HSNDT [17,44,56–59], and Carrera Unified Formulation (CUF) [60,61]. For instance, Singh and Rao [54], using FSDT, pointed out the importance of full Green-Lagrange nonlinearity in comparison to von Kármán nonlinearity, for the thick laminated plates. Their study shows that the addition of extra nonlinear term in the strain displacement relation affects the central deflection by 13%. Le-Manh et al. [55] studied the nonlinear behavior of composite plate by considering large displacement, large in-plane strain, and small rotations via isogeometric analysis associated with FSDT. The study shows the importance of Green-Lagrange strain with small rotation over von Kármán strain in complex boundary conditions using FSDT. Wu et al. [60] proposed a full geometric nonlinear plate model using Carrera Unified Formulation (CUF) for isotropic rectangular plates via means of Total Lagrangian approach. They have also shown that von Kármán and Green-Lagrange results are only consistent in loads with small magnitude for a moderately thick isotropic plate. Note that, in the aforementioned papers on nonlinear bending analysis of laminated composite plates, the application of Green-Lagrange nonlinearity is limited to plates with all edges subjected to some boundary constraints. However, in aerospace, automobile, and others, where plates are allowed to move freely, having no geometric boundary conditions, are highly prevalent. The only available paper in this regard is by Le-Manh et al. [55] which considers the one free edge plate with the remaining three sides subjected to immovable boundary conditions using FSDT in conjunction with small rotation Green-Lagrange nonlinearity. Moreover, no paper is available which utilizes TSDT or NPSDT with Green-Lagrange nonlinearity for nonlinear analysis despite the defused popularity of TSDT and various developed NPSDTs for laminated plates. Further, as per authors' best knowledge, the need of Green-Lagrange nonlinearity over von Kármán nonlinearity in bending analysis is not established despite of various studies have been carried out through Green-Lagrange nonlinearity.

In comparison to the laminated plate, very few studies have been conducted on the sandwich composite plate for nonlinear analysis [62–67]. For instance, That-Hong et al. [65] formulated a four-noded quadrilateral plate element by combining cell-based smoothed strain with TSDT for geometrically nonlinear analysis. Note that, in the aforementioned papers [62–66] higher-order shear deformation theory, particularly TSDT, was used for modeling the plate displacements. However, as per authors' best knowledge, the literature on the application of NPSDT for nonlinear bending analysis of the sandwich plate is scarcely available.

From the concise literature reviewed above, it can be noticed that the geometrically nonlinear behavior of laminated composite structures has been extensively studied by different numerical methods. Among them, FEM is the most preferred tool to study structural behavior due to its popular and well established mathematical background. However, most FEM studies have been limited to von Kármán's sense of nonlinearity, while very few studies have been reported with Green-Lagrange nonlinearity. As per authors' knowledge, despite the development of various new non-polynomial shear deformation theories (NPSDTs) [3,4], no literature has been reported on nonlinear static analysis using NPSDT with full geometric nonlinearity. Thus, it is essential to conduct a study to get a clear understanding of the efficiency of these newly developed NPSDTs for nonlinear static analysis. Moreover, it is observed in the literature that the accuracy of NPSDT for anti-symmetric cross-ply is severely lacking.

In this paper, we have illustrated the importance of Green-Lagrange nonlinearity over von Kármán nonlinearity for nonlinear bending analysis of multilayered composite plate through a rigorous comparison study. For comparison, various boundary conditions such as movable and immovable simply supported, and hinged boundary conditions with and without rotation are considered at different load amplitudes. Further, this same comparison is carried out for a plate with one free edge. An energy approach is utilized to formulate the weak form of the equilibrium equations. For kinematic modeling of the plate, both TSDT and IHSDT in the framework of generalized higher-order shear deformation theory (HSDT) are considered and then discretized using a nine-noded penalty based C^0 finite element.

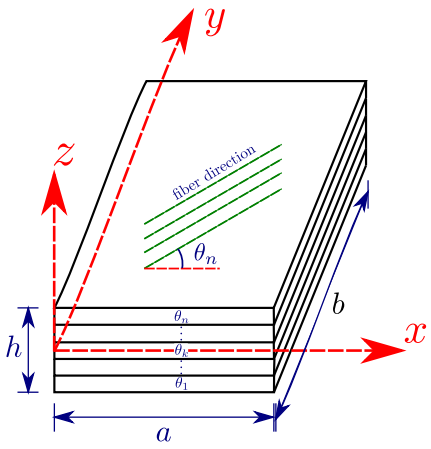

Fig. 1. Schematic diagram of multilayered composite plate with $x-y-z$ Cartesian coordinate system.

Then, the obtained set of nonlinear equations is incrementally solved via Newton-Raphson method. The results reveal that the performance of IHSDT and TSDT is found to be better in the symmetric and anti-symmetric cross-ply laminated plates, respectively. Further, the penalty parameter has a prevailing impact on the accuracy of the thick anti-symmetric cross-ply laminated plate and less effect on the symmetric cross-ply laminated plate. The present study suggests the use of Green-Lagrange nonlinearity for nonlinear bending analysis of multilayered composite plate subjected to in-plane movable (normal) displacement constraint for better prediction of the structural response.

The rest of the paper is organized as follows. Section 2 describes the mathematical formulation. In Section 3, the set of governing equations is derived in the finite element context. In Section 4, the accuracy of the present method is established by comparing the obtained results with those available in the literature and results obtained by ANSYS for thin isotropic plates and for thin and thick laminated plates subjected to different boundary condition with one free edge. Subsequently, parametric studies considering various side-to-thickness ratio, number of layers, and fiber orientation are presented for in-plane movable (normal) simply supported boundary condition. In Section 5, a conclusion is drawn based on this study which suggests the use of Green-Lagrange nonlinearity for analysis when structure possesses in-plane movable (normal) simply supported condition or free edge/s.

2. Mathematical formulation

A rectangular multilayered composite plate composed of n elastic orthotropic layers stacked in particular sequence $(\theta_1/\theta_2/\theta_3/\theta_4/\ldots/\theta_n)$ is considered. The plate dimensions are named as length a, width b, and uniform thickness h. A Cartesian coordinate system, with $x-y$ plane coinciding with middle plane of the plate, is chosen as shown in Fig. 1.

2.1. Higher-order shear deformation theory

Based on the characteristics of equivalent higher-order shear deformation theory with five field variables [2], the assumed displacement field can be defined in general form as follows:

$$\begin{aligned} u(x,y,z) &= u_0(x,y) - z\frac{\partial w_0}{\partial x} + f(z)\,\theta_x(x,y) \\ v(x,y,z) &= v_0(x,y) - z\frac{\partial w_0}{\partial y} + f(z)\,\theta_y(x,y) \\ w(x,y,z) &= w_0(x,y) \end{aligned} \tag{1}$$

where, u, v, and w are the displacements of arbitrary point in x, y, z directions, respectively; u_0, v_0, and w_0 denote the midplane displacements, respectively; θ_x and θ_y represent the shear deformation of midplane normal about y-axis and x-axis, respectively; and $f(z)$ is a thickness function. If thickness function, $f(z)$ is a polynomial or non-polynomial function of z, then the theory is named as polynomial (PSDT) or non-polynomial shear deformation theory (NPSDT), respectively. Usually, the function, $f(z)$ is such that it satisfy zero transverse shear deformation at the top and bottom surfaces of the plate.

As pointed out in the introduction section, most displacement based finite element models use Lagrange basis function which satisfy only C^0 continuity of the field variables. As approximating the solution for C^1 continuity with Hermite basis function has its own difficulty in implementation of finite element code [68]. To formulate the finite element model with HSDT (given in Eq. (2)) using Lagrange element, an artificial field variables need to be considered which in turn reduces the required continuity to C^0. This conversion is compensated by penalty constraints on the strain energy [69] shown in following subsection. Considering the above assumption, HSDT now contains seven field variables, $\{\boldsymbol{u}\} = \{u_0,\ v_0,\ w_0,\ \phi_x = -\frac{\partial w_0}{\partial x},\ \phi_y = -\frac{\partial w_0}{\partial y},\ \theta_x,\ \theta_y\}^T$ and same is expressed as:

$$\begin{aligned} u(x,y,z) &= u_0(x,y) + z\phi_x + f(z)\,\theta_x(x,y) \\ v(x,y,z) &= v_0(x,y) + z\phi_y + f(z)\,\theta_y(x,y) \\ w(x,y,z) &= w_0(x,y) \end{aligned} \tag{2}$$

2.2. Strain-displacement relation

The state of strain, $\boldsymbol{\varepsilon}$ at a point, using Green-Lagrange strain relation, is given by following expression:

$$\boldsymbol{\varepsilon} = \begin{Bmatrix} \frac{\partial u}{\partial x} \\ \frac{\partial v}{\partial y} \\ \frac{\partial u}{\partial y} + \frac{\partial v}{\partial x} \\ \frac{\partial v}{\partial z} + \frac{\partial w}{\partial y} \\ \frac{\partial u}{\partial z} + \frac{\partial w}{\partial x} \end{Bmatrix} + \frac{1}{2} \begin{Bmatrix} \left(\frac{\partial u}{\partial x}\right)^2 + \left(\frac{\partial v}{\partial x}\right)^2 + \left(\frac{\partial w}{\partial x}\right)^2 \\ \left(\frac{\partial u}{\partial y}\right)^2 + \left(\frac{\partial v}{\partial y}\right)^2 + \left(\frac{\partial w}{\partial y}\right)^2 \\ 2\left(\frac{\partial u}{\partial x}\frac{\partial u}{\partial y} + \frac{\partial v}{\partial x}\frac{\partial v}{\partial y} + \frac{\partial w}{\partial x}\frac{\partial w}{\partial y}\right) \\ 2\left(\frac{\partial u}{\partial y}\frac{\partial u}{\partial z} + \frac{\partial v}{\partial y}\frac{\partial v}{\partial z} + \frac{\partial w}{\partial y}\frac{\partial w}{\partial z}\right) \\ 2\left(\frac{\partial u}{\partial x}\frac{\partial u}{\partial z} + \frac{\partial v}{\partial x}\frac{\partial v}{\partial z} + \frac{\partial w}{\partial x}\frac{\partial w}{\partial z}\right) \end{Bmatrix} = \boldsymbol{\varepsilon_l} + \frac{1}{2}\boldsymbol{\varepsilon_{nl}} \tag{3}$$

whereas, von Kármán strain relation is given as follows:

$$\boldsymbol{\varepsilon} = \begin{Bmatrix} \frac{\partial u}{\partial x} \\ \frac{\partial v}{\partial y} \\ \frac{\partial u}{\partial y} + \frac{\partial v}{\partial x} \\ \frac{\partial v}{\partial z} + \frac{\partial w}{\partial y} \\ \frac{\partial u}{\partial z} + \frac{\partial w}{\partial x} \end{Bmatrix} + \frac{1}{2} \begin{Bmatrix} \left(\frac{\partial w}{\partial x}\right)^2 \\ \left(\frac{\partial w}{\partial y}\right)^2 \\ 2\left(\frac{\partial w}{\partial x}\frac{\partial w}{\partial y}\right) \\ 0 \\ 0 \end{Bmatrix} = \boldsymbol{\varepsilon_l} + \frac{1}{2}\boldsymbol{\varepsilon_{nl}} \tag{4}$$

By substituting the relation of modified displacement from Eq. (2) in Eq. (3), linear strain vector, $\boldsymbol{\varepsilon}_l$ can be rewritten as:

$$\boldsymbol{\varepsilon}_l = \begin{Bmatrix} \boldsymbol{\varepsilon}_{lb} \\ \boldsymbol{\varepsilon}_{ls} \end{Bmatrix} = \begin{Bmatrix} \boldsymbol{Z}_{lb}\hat{\boldsymbol{\varepsilon}}_{lb} \\ \boldsymbol{Z}_{ls}\hat{\boldsymbol{\varepsilon}}_{ls} \end{Bmatrix} \tag{5}$$

in which

$$\hat{\boldsymbol{\varepsilon}}_{lb} = \left\{ \frac{\partial u_0}{\partial x} \;\; \frac{\partial v_0}{\partial y} \;\; \frac{\partial u_0}{\partial y} + \frac{\partial v_0}{\partial x} \;\; \frac{\partial \phi_x}{\partial x} \;\; \frac{\partial \phi_y}{\partial y} \;\; \frac{\partial \phi_x}{\partial y} + \frac{\partial \phi_y}{\partial x} \;\; \frac{\partial \theta_x}{\partial x} \;\; \frac{\partial \theta_y}{\partial y} \;\; \frac{\partial \theta_x}{\partial y} + \frac{\partial \theta_y}{\partial x} \right\}^T ; \;\; \boldsymbol{Z}_{lb} = \begin{bmatrix} 1 & 0 & 0 & z & 0 & 0 & f(z) & 0 & 0 \\ 0 & 1 & 0 & 0 & z & 0 & 0 & f(z) & 0 \\ 0 & 0 & 1 & 0 & 0 & z & 0 & 0 & f(z) \end{bmatrix} \tag{6a}$$

$$\hat{\boldsymbol{\varepsilon}}_{ls} = \left\{ \frac{\partial w_0}{\partial y} + \phi_y \;\; \frac{\partial w_0}{\partial x} + \phi_x \;\; \theta_y \;\; \theta_x \right\}^T ; \;\; \boldsymbol{Z}_{ls} = \begin{bmatrix} 1 & 0 & f'(z) & 0 \\ 0 & 1 & 0 & f'(z) \end{bmatrix} \tag{6b}$$

Similarly, nonlinear strain vector, $\boldsymbol{\varepsilon}_{nl}$ can be reorganized as follows:

$$\boldsymbol{\varepsilon}_{nl} = \begin{Bmatrix} \boldsymbol{\varepsilon}_{nlb} \\ \boldsymbol{\varepsilon}_{nls} \end{Bmatrix} = \begin{Bmatrix} \boldsymbol{Z}_{nlb}\hat{\boldsymbol{\varepsilon}}_{nlb} \\ \boldsymbol{Z}_{nls}\hat{\boldsymbol{\varepsilon}}_{nls} \end{Bmatrix} = \begin{Bmatrix} \boldsymbol{Z}_{nlb}\boldsymbol{A}_b\boldsymbol{\phi}_b \\ \boldsymbol{Z}_{nls}\boldsymbol{A}_s\boldsymbol{\phi}_s \end{Bmatrix} \tag{7}$$

in which

$$\boldsymbol{Z}_{nlb} = \begin{bmatrix} 1 & 0 & 0 & z & 0 & 0 & f(z) & 0 & 0 & z^2 & 0 & 0 & zf(z) & 0 & 0 & (f(z))^2 & 0 & 0 \\ 0 & 1 & 0 & 0 & z & 0 & 0 & f(z) & 0 & 0 & z^2 & 0 & 0 & zf(z) & 0 & 0 & (f(z))^2 & 0 \\ 0 & 0 & 1 & 0 & 0 & z & 0 & 0 & f(z) & 0 & 0 & z^2 & 0 & 0 & zf(z) & 0 & 0 & (f(z))^2 \end{bmatrix} \tag{8a}$$

$$\boldsymbol{Z}_{nls} = \begin{bmatrix} 1 & 0 & z & 0 & f(z) & 0 & f'(z) & 0 & zf'(z) & 0 & f(z)f'(z) & 0 \\ 0 & 1 & 0 & z & 0 & f(z) & 0 & f'(z) & 0 & zf'(z) & 0 & f(z)f'(z) \end{bmatrix} \tag{8b}$$

$$\boldsymbol{\phi}_b = \left\{ \frac{\partial u_0}{\partial x} \;\; \frac{\partial u_0}{\partial y} \;\; \frac{\partial v_0}{\partial x} \;\; \frac{\partial v_0}{\partial y} \;\; \frac{\partial w_0}{\partial x} \;\; \frac{\partial w_0}{\partial y} \;\; \frac{\partial \phi_x}{\partial x} \;\; \frac{\partial \phi_x}{\partial y} \;\; \frac{\partial \phi_y}{\partial x} \;\; \frac{\partial \phi_y}{\partial y} \;\; \frac{\partial \theta_x}{\partial x} \;\; \frac{\partial \theta_x}{\partial y} \;\; \frac{\partial \theta_y}{\partial x} \;\; \frac{\partial \theta_y}{\partial y} \right\}^T \tag{8c}$$

$$\boldsymbol{\phi}_s = \left\{ \phi_x \;\; \phi_y \;\; \theta_x \;\; \theta_y \;\; \frac{\partial u_0}{\partial x} \;\; \frac{\partial u_0}{\partial y} \;\; \frac{\partial v_0}{\partial x} \;\; \frac{\partial v_0}{\partial y} \;\; \frac{\partial \phi_x}{\partial x} \;\; \frac{\partial \phi_x}{\partial y} \;\; \frac{\partial \phi_y}{\partial x} \;\; \frac{\partial \phi_y}{\partial y} \;\; \frac{\partial \theta_x}{\partial x} \;\; \frac{\partial \theta_x}{\partial y} \;\; \frac{\partial \theta_y}{\partial x} \;\; \frac{\partial \theta_y}{\partial y} \right\}^T \tag{8d}$$

2.3. Constitutive relation

The constitutive relation for kth layer of multilayered plate can be expressed in $x-y-z$ global coordinate system as:

$$\begin{Bmatrix} \sigma_{xx} \\ \sigma_{yy} \\ \tau_{xy} \end{Bmatrix} = \begin{bmatrix} \bar{Q}_{11} & \bar{Q}_{12} & \bar{Q}_{16} \\ \bar{Q}_{12} & \bar{Q}_{22} & \bar{Q}_{26} \\ \bar{Q}_{16} & \bar{Q}_{26} & \bar{Q}_{66} \end{bmatrix} \begin{Bmatrix} \varepsilon_{xx} \\ \varepsilon_{yy} \\ \gamma_{xy} \end{Bmatrix} \quad \text{and} \quad \begin{Bmatrix} \tau_{yz} \\ \tau_{xz} \end{Bmatrix} = \begin{bmatrix} \bar{Q}_{44} & \bar{Q}_{45} \\ \bar{Q}_{45} & \bar{Q}_{55} \end{bmatrix} \begin{Bmatrix} \gamma_{yz} \\ \gamma_{xz} \end{Bmatrix}$$

where $(\sigma_{xx}, \sigma_{yy}, \tau_{xy}, \tau_{yz}, \tau_{xz})$ are the stress and $(\varepsilon_{xx}, \varepsilon_{yy}, \gamma_{xy}, \gamma_{yz}, \gamma_{xz})$ are the strain components of the k^{th} ply in the global coordinates, and $\bar{Q}_{ij}$ are the transformed material constants with local coordinates at θ_k angle about z-axis as shown in Fig. 1. The expression of $\bar{Q}_{ij}$ in terms of material constants in global coordinate system can be found in any standard finite element textbook such as [69].

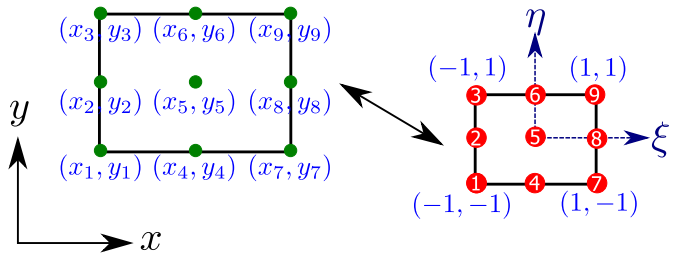

Fig. 2. Nine-noded isoparametric element.

Consequently, the inplane stress resultant and the transverse shear resultants are defined as:

$$\begin{bmatrix} N_{xx} & M_{xx} & P_{xx} & Q_{xx} & R_{xx} & S_{xx} \\ N_{yy} & M_{yy} & P_{yy} & Q_{yy} & R_{yy} & S_{yy} \\ N_{xy} & M_{xy} & P_{xy} & Q_{xy} & R_{xy} & S_{xy} \end{bmatrix} = \int_{-h/2}^{h/2} \begin{Bmatrix} \sigma_{xx} \\ \sigma_{yy} \\ \tau_{xy} \end{Bmatrix} \left\{ 1 \;\; z \;\; f(z) \;\; z^2 \;\; zf(z) \;\; f^2(z) \right\} dz \tag{9a}$$

$$\begin{bmatrix} N_{yz} & M_{yz} & P_{yz} & Q_{yz} & R_{yz} & S_{yz} \\ N_{xz} & M_{xz} & P_{xz} & Q_{xz} & R_{xz} & S_{xz} \end{bmatrix} = \int_{-h/2}^{h/2} \begin{Bmatrix} \tau_{yz} \\ \tau_{xz} \end{Bmatrix} \left\{ 1 \;\; z \;\; f(z) \;\; f'(z) \;\; zf'(z) \;\; f(z) f'(z) \right\} dz \tag{9b}$$

2.4. Variational principle

For arbitrary space variable and admissible virtual displacement $\delta\{u, v, w\}$, principle of virtual work for given system, using total Lagrangian approach, is given as:

$$\int_V \left[\delta\{\boldsymbol{\varepsilon}\}^T \{\boldsymbol{\sigma}\} + \delta \left(\frac{\partial w_0}{\partial x} + \phi_x \right)^T \gamma \left(\frac{\partial w_0}{\partial x} + \phi_x \right) + \delta \left(\frac{\partial w_0}{\partial y} + \phi_y \right)^T \gamma \left(\frac{\partial w_0}{\partial y} + \phi_y \right) \right] dV = \int_A \delta w^T P dA \tag{10}$$

where, γ represents the penalty parameter for artificial constraints, and the term associated with γ is followed from penalty function method for constrained problem [1,15,69].

Here, all the kinematics and stress variables are measured with respect to undeformed configuration (i.e., Total Lagrangian approach).

The first term in the Eq. (10) represents virtual strain energy and is written in expanded form as:

$$\delta U = \int_V (\delta\boldsymbol{\varepsilon})^T \boldsymbol{\sigma} dz dA = \int_V (\delta\boldsymbol{\varepsilon}_l + \delta\boldsymbol{\varepsilon}_{nl}) \bar{Q} \left(\boldsymbol{\varepsilon}_l + \frac{1}{2}\boldsymbol{\varepsilon}_{nl} \right) dz dA \tag{11a}$$

$$= \int_V \left\{ (\delta\hat{\boldsymbol{\varepsilon}}_l)^T \boldsymbol{Z}_l^T \bar{Q} \boldsymbol{Z}_l \hat{\boldsymbol{\varepsilon}}_l + \frac{1}{2} (\delta\hat{\boldsymbol{\varepsilon}}_l)^T \boldsymbol{Z}_l^T \bar{Q} \boldsymbol{Z}_{nl} \hat{\boldsymbol{\varepsilon}}_{nl} + (\delta\hat{\boldsymbol{\varepsilon}}_{nl})^T \boldsymbol{Z}_{nl}^T \bar{Q} \boldsymbol{Z}_l \hat{\boldsymbol{\varepsilon}}_l + \frac{1}{2} (\delta\hat{\boldsymbol{\varepsilon}}_{nl})^T \boldsymbol{Z}_{nl}^T \bar{Q} \boldsymbol{Z}_{nl} \hat{\boldsymbol{\varepsilon}}_{nl} \right\} dz dA \tag{11b}$$

The second and third terms in the Eq. (10) represent strain energy due to artificial constraints, and the combined expression is

$$\delta U_\gamma = \int_V \gamma \left[\delta \left(\frac{\partial w_0}{\partial x} + \phi_x \right)^T \left(\frac{\partial w_0}{\partial x} + \phi_x \right) + \delta \left(\frac{\partial w_0}{\partial y} + \phi_y \right)^T \left(\frac{\partial w_0}{\partial y} + \phi_y \right) \right] dz dA \tag{12}$$

The last term of Eq. (10) represents virtual work done by transverse mechanical load and is expressed as

$$\delta W_{ext} = \int_A \delta w_0 P(x, y)|_{z=h/2} dA \tag{13}$$

Here, $P(x, y)|_{z=h/2}$ represents spatially distributed transverse load acting on the top surface ($z = h/2$). For simplicity, the external load is considered as non-follower load, and it does not change with the deformation of the plate.

3. Finite element formulation

In finite element method, plate domain (geometry) is need to be discretized to form a mesh of finite elements connected through nodes. In this study, a nine-noded isoparametric Lagrange element is considered (shown in Fig. 2).

Following the definition of shape function from geometric description, the displacement field variables (in Eq. (2)) are interpolated at arbitrary point (x, y) as:

$$x = \sum_{i=1}^{9} N_i x_i; \quad y = \sum_{i=1}^{9} N_i y_i; \quad \{\boldsymbol{u}\} = \sum_{i=1}^{9} [I_7] N_i \{\boldsymbol{q}_i\} \tag{14}$$

Here, $[I_7]$ denotes an identity matrix of order 7 and $\boldsymbol{q}_i$ denotes vector of seven nodal displacement field variables or degree of freedom, i.e., $\{\boldsymbol{q}_i\} = \{u_{0i},\ v_{0i},\ w_{0i},\ \phi_{xi},\ \phi_{yi},\ \theta_{xi},\ \theta_{yi}\}^T$ corresponding to i^{th} node with i^{th} shape function, N_i.

The expressions for shape functions, corresponding to nodes shown in Fig. 2, are as follows:

$$N_1 = \frac{1}{4}\xi\eta\,(\xi-1)\,(\eta-1)\,; \qquad N_4 = -\frac{1}{2}\left(\xi^2-1\right)(\eta-1)\,\eta; \quad N_7 = \frac{1}{4}\xi\,(\xi+1)\,\eta\,(\eta-1)$$
$$N_2 = -\frac{1}{2}\xi\,(\xi-1)\left(\eta^2-1\right); \quad N_5 = \left(\xi^2-1\right)\left(\eta^2-1\right); \qquad N_8 = -\frac{1}{2}\xi\,(\xi+1)\left(\eta^2-1\right)$$
$$N_3 = \frac{1}{4}\xi\eta\,(\xi-1)\,(\eta+1)\,; \qquad N_6 = -\frac{1}{2}\left(\xi^2-1\right)\eta\,(\eta+1)\,; \quad N_9 = \frac{1}{4}\xi\,(\xi+1)\,\eta\,(\eta+1)$$

By substituting Eq. (14) in Eqs. (6) and (8), and with this generalized strain vector, $\hat{\boldsymbol{\varepsilon}}$ can be rewritten in terms of strain displacement matrix, $\boldsymbol{B}$ and elemental displacement vector, $\boldsymbol{q}$. Here, for ease in implementation of finite element formulation/code, the bending and transverse shear parts are considered separately, which are uncoupled in multilayered orthotropic composite; and the same is symbolically expressed as:

$$\hat{\boldsymbol{\varepsilon}}_{lj} = \sum_{i=1}^{9} \boldsymbol{B}^L_{ji}\boldsymbol{q}_i = \boldsymbol{B}^L_j\boldsymbol{q}; \quad \hat{\boldsymbol{\varepsilon}}_{nlj} = \sum_{i=1}^{9} \boldsymbol{A}_j\boldsymbol{G}^{NL}_{ji}\boldsymbol{q}_j = \sum_{i=1}^{9} \boldsymbol{B}^{NL}_{ji}\boldsymbol{q}_i = \boldsymbol{B}^{NL}_j\boldsymbol{q}$$
$$\boldsymbol{q} = \left\{\ \boldsymbol{q}_1^T\ \ \boldsymbol{q}_2^T\ \ \cdots\ \ \boldsymbol{q}_8^T\ \ \boldsymbol{q}_9^T\ \right\}^T \tag{15}$$

where, $j = 'b'$ for bending and $j = 's'$ for transverse shear part; while superscript L represents the linear part, and superscript NL represents the nonlinear part.

So the explicit expression of $\boldsymbol{B}^L_j$ and $\boldsymbol{B}^{NL}_j$ contains terms which require first Cartesian derivative of Lagrange basis function, $\left(\frac{\partial N_i}{\partial x}\right)$. Using chain-rule, first derivative of N_i (in Cartesian coordinate) can be calculated in terms of derivative with respect to parametric coordinate (ξ and η) by following relation:

$$\begin{Bmatrix} \frac{\partial N_i}{\partial x} \\ \frac{\partial N_i}{\partial y} \end{Bmatrix} = \begin{bmatrix} \frac{\partial x}{\partial \xi} & \frac{\partial y}{\partial \xi} \\ \frac{\partial x}{\partial \eta} & \frac{\partial y}{\partial \eta} \end{bmatrix}^{-1} \begin{Bmatrix} \frac{\partial N_i}{\partial \xi} \\ \frac{\partial N_i}{\partial \eta} \end{Bmatrix}$$

Similarly, strain-displacement matrix for Eq. (12) can also be obtained in similar manner and virtual strain energy due to penalty can be rewritten as:

$$\delta U_\gamma = (\delta\boldsymbol{q})^T \int_V \left[\boldsymbol{B}_\gamma\right]^T \left[\boldsymbol{B}_\gamma\right] \gamma\, dz dA \tag{16}$$

3.1. System of equations

By utilizing Eqs. (14) and (15) in Eqs. (11), (13) and (16) with followed substitution into Eq. (10) and then eliminating the virtual displacement vector, $(\delta\boldsymbol{q})^T$; the set of equations for static analysis under distributed transverse load is obtained as:

$$\left(\boldsymbol{K} + \gamma\,\boldsymbol{K}_\gamma\right)\boldsymbol{q} = \boldsymbol{F}_P \tag{17}$$

in which

$$\boldsymbol{K} = \int_V \left(\left(\boldsymbol{B}^L\right)^T \boldsymbol{Z}_l^T\,\bar{\mathbf{Q}}\,\boldsymbol{Z}_l\boldsymbol{B}^L + \frac{1}{2}\left(\boldsymbol{B}^L\right)^T \boldsymbol{Z}_l^T\,\bar{\mathbf{Q}}\,\boldsymbol{Z}_{nl}\boldsymbol{B}^{NL} + \left(\boldsymbol{B}^{NL}\right)^T \boldsymbol{Z}_{nl}^T\,\bar{\mathbf{Q}}\,\boldsymbol{Z}_l\boldsymbol{B}^L + \frac{1}{2}\left(\boldsymbol{B}^{NL}\right)^T \boldsymbol{Z}_{nl}^T\,\bar{\mathbf{Q}}\,\boldsymbol{Z}_{nl}\boldsymbol{B}^{NL} \right) dz dA$$
$$\boldsymbol{K}_\gamma = \int_V \left[\boldsymbol{B}_\gamma\right]^T \left[\boldsymbol{B}_\gamma\right] dz dA; \quad \boldsymbol{F}_P = \int_A \{\mathscr{W}\}\, P\,(x,y)\, dA$$

where

$$\{\mathscr{W}\}\{\boldsymbol{q}\} = \sum_{i=1}^{9} \{\mathscr{W}_i\}\boldsymbol{q}_i; \quad \{\mathscr{W}_i\} = \left\{\ 0\ \ 0\ \ N_i\ \ 0\ \ 0\ \ 0\ \ 0\ \right\}$$

3.2. Solution procedure

In this section, solution procedure for nonlinear algebraic equations, Eq. (17) is discussed. After assembling elemental set of equation for all finite elements and imposing the suitable boundary conditions, the nonlinear system of algebraic equations is solved iteratively. There are several iterative approaches to solve these nonlinear sets of equations and the fundamental impetus behind these approaches is the residual due to the assumed solution.

As present study is confined to plate structure only, subjected to transverse load, which generally do not exhibit snap-back and snap-through behavior. Thus, for nonlinear static analysis, Newton-Raphson iterative method is employed to obtain the solution for the discrete incremental mechanical load step. For each incremental load, the incremental change in the displacement, $\Delta\boldsymbol{q}$ can be defined for n^{th} iteration:

$$\Delta \boldsymbol{q} = \frac{\left(\boldsymbol{F}_P - \left(\boldsymbol{K}\left(\boldsymbol{q}_n\right) - \gamma \boldsymbol{K}_\gamma\right)\boldsymbol{q}_n\right)}{\boldsymbol{K}_T}$$

where, $\boldsymbol{K}_T$ is the tangent stiffness matrix and is defined as

$$\boldsymbol{K}_T = \gamma \boldsymbol{K}_\gamma + \boldsymbol{K}_L + \boldsymbol{K}_{NL} + \boldsymbol{K}_\sigma$$

Herein, $\boldsymbol{K}_\sigma = \int_A \left\{ \left(\boldsymbol{G}_{bj}^{NL}\right)^T \mathbb{N}_b \boldsymbol{G}_{bj}^{NL} + \left(\boldsymbol{G}_{sj}^{NL}\right)^T \mathbb{N}_s \boldsymbol{G}_{sj}^{NL} \right\} dA$ in which expression of $\mathbb{N}_b$ and $\mathbb{N}_s$ are given in the Appendix A and the combined expression for $\boldsymbol{K}_L + \boldsymbol{K}_{NL}$ is given by Eq. (19).

$$\boldsymbol{K}_L + \boldsymbol{K}_{NL} = \int_V \left[\left\{ \left(\boldsymbol{B}^L\right)^T \boldsymbol{Z}_l^T + \left(\boldsymbol{B}^{NL}\right)^T \boldsymbol{Z}_{nl}^T \right\} \bar{\boldsymbol{Q}} \left\{ \boldsymbol{Z}_l \boldsymbol{B}^L + \boldsymbol{Z}_{nl} \boldsymbol{B}^{NL} \right\} \right] dz dA \tag{19}$$

The process is repeated until the convergence criterion is satisfied. Here, a relative displacement norm criterion:

$$\frac{||\Delta \boldsymbol{q}||}{||\boldsymbol{q}||} < \beta$$

is used with error tolerance, $\beta = 10^{-2}$ or otherwise stated in the problem.

3.3. Stress-recovery technique over the surface

In this subsection, the stress-recovery technique [70,71] used to obtain the continuous and improved stress component over the surface is briefly discussed. It is found in the literature that the performance of super convergent patch recovery (SPR) is superior than its counter part, i.e., direct interpolation and continuous least square projection (CL2P) techniques [71]. Here, in this study, a SPR technique is applied only to recover the inplane distribution of stresses.

In general, the inplane distribution of stresses is smooth and continuous for bending problem as observed in 3D elasticity solution [69]. However, due to the consideration of C^0 continuous Lagrange element as in the present finite element model, only primary solution, i.e., displacement is found to be continuous over the plate. Particularly, from the viewpoint of designer or engineer, an accurate distribution of stresses is of more importance than the displacement. In order to obtain smooth and continuous stresses over the plate surface, a stress-recovery technique is needed to be used in the post-processing step to obtain the accurate inplane distribution of stresses.

Moreover, the through-thickness distribution of transverse stresses, τ_{yz} and τ_{xz} predicted by present FEM model is also found to be continuous due to HSDT [69]. Also, it is well established in the literature that the accurate distribution of transverse stresses is possible through integration of 3D elasticity equilibrium equations [69,72,73]. However, this approach requires second derivative of primary solution which is less accurate or constant for lower finite element [74]. Hence, different researchers have used different techniques to obtain the second derivative of displacement [72,73,75]. Further, the transverse stresses obtained through the constitutive relation employing HSDT give reasonably good idea about the through-thickness variation of transverse stresses. Hence, for present study, no recovery technique is used in thickness direction, and transverse stresses are obtained through the constitutive relation for both von Kármán and Green-Lagrange non-linearity. It is shown in the Section 4 that the use of constitutive approach for transverse stresses is limited to von Kármán non-linearity only and is not useful for Green-Lagrange nonlinearity, and the use of equilibrium approach in the thickness direction is suggested, as done in references [72,73,75].

In SPR technique [71], the improved stress components, σ^* are obtained by taking a least square projection of the computed stress, σ at sampling (Gauss-Legendre) points over a patch. Here, a patch is defined as group of elements with vertex node at its center. A patch can contain three or more elements and can be classified as interior or boundary patch accordingly as shown in Figs. 3a and 3b.

In order to obtain the continuous improved stresses over the patch for each stress component, the improved stress field, σ^* is assumed to be a form of polynomial expansion. In present study, the polynomial expansion written in Eq. (20) is considered for modeling.

$$\sigma^* = P_0 + \bar{x}P_1 + \bar{y}P_2 + \bar{x}\bar{y}P_3 + \bar{x}^2 P_4 + \bar{y}^2 P_5 + \bar{x}^2\bar{y}P_6 + \bar{x}\bar{y}^2 P_7 + \bar{x}^2\bar{y}^2 P_8 \tag{20}$$

or

$$\sigma^* = \mathscr{M}_i P_i = \mathscr{M}\boldsymbol{P}$$

where, P_i is the unknown coefficient to be determined for each stress component in a patch with $\bar{x} = x_{sp} - x_v$ and $\bar{y} = y_{sp} - y_v$. Here, x_{sp} and x_v represent the x-coordinate of sampling and vertex points, respectively.

It is to be noted that any suitable polynomial expansion can be considered according to the number of sampling points and number of unknown coefficients taken in a single patch. As stated above, the unknown expansion coefficients are determined by making it fit the calculated stresses at the set of sampling points inside the patch in a least square manner which is defined as

$$\mathscr{F} = \frac{1}{2}\left(\sigma^* - \sigma\right)^T \left(\sigma^* - \sigma\right) d\Omega_p$$

$$\int_{\Omega_p} \frac{\partial \mathscr{F}}{\partial P_i} = \int_{\Omega_p} \left(\frac{\partial \sigma^*}{\partial P_i}\right)^T \left(\sigma^* - \sigma\right) d\Omega_p = 0$$

or

$$\int_{\Omega_p} \mathscr{M}^T \mathscr{M} d\Omega_p \boldsymbol{P} = \int_{\Omega_p} \mathscr{M}^T \sigma \, d\Omega_p \text{ or } \boldsymbol{A}\boldsymbol{P} = \boldsymbol{B}$$

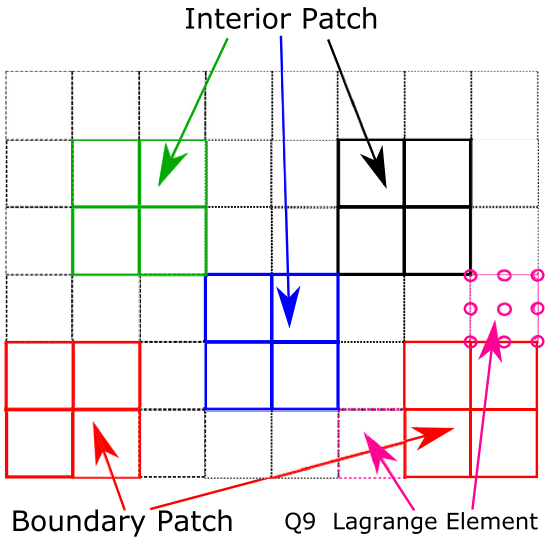

(a) Interior and boundary patches.

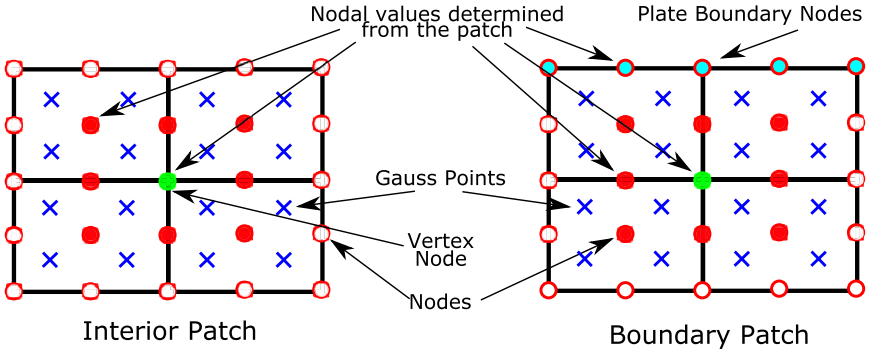

(b) Four-element patch.

Fig. 3. SPR patch for Q9 Lagrange element. (For interpretation of the colors in the figure(s), the reader is referred to the web version of this article.)

in which,

$$\boldsymbol{A} = \int_{\Omega_p} \mathscr{M}^T \mathscr{M} d\Omega_p \text{ and } \boldsymbol{B} = \int_{\Omega_p} \mathscr{M}^T \sigma d\Omega_p$$

Here, the symbol Ω_p represents the patch domain. After solving for the unknown coefficient, P_i for each stress component, the required stress value at selected nodes (see 3b) can be obtained using Eq. (20). In this SPR approach, some nodes can have multiple values due to the overlapping of patches as depicted in Fig. 4. Hence, a simple averaging is needed to reach a unique stress value over the surface.

4. Numerical results and discussions

In this section, the accuracy and efficacy of the present C^0 finite element formulation are assessed through several nonlinear bending examples along with the effect of penalty constraints. Also, numerical results obtained using present formulation for PSDT (specifically TSDT), $f(z) = z - 4z^3/3h^2$ [18,69] and NPSDT (specifically IHSDT), $f(z) = sinh^{-1}(3z/h) - 6z/h\sqrt{13}$ [5] are studied comparatively. Both present solutions are further compared with obtained ANSYS solutions and other analytical, experimental, and numerical solutions from the literature. The present NPSDT, i.e., IHSDT is selected based on its analytical and numerical performance over other theories shown in the references [1,2,5,6,15].

4.1. Material properties

The following sets of material properties are used in subsequent section:

- Material-I: [55]
  $E_1/E_2 = 25$, $G_{12}/E_2 = G_{13}/E_2 = 0.5$, $G_{23}/E_2 = 0.2$, $\nu_{12} = 0.25$
- Material-II: [69]
  $E_1/E_2 = 40$ or variable, $G_{12}/E_2 = G_{13}/E_2 = 0.6$, $G_{23}/E_2 = 0.5$, $\nu_{12} = 0.25$
- Material-III: [18,29]
  $E_1 = 3 \times 10^6$ psi (20.684 GPa), $E_2 = 1.28 \times 10^6$ psi (8.825 GPa),

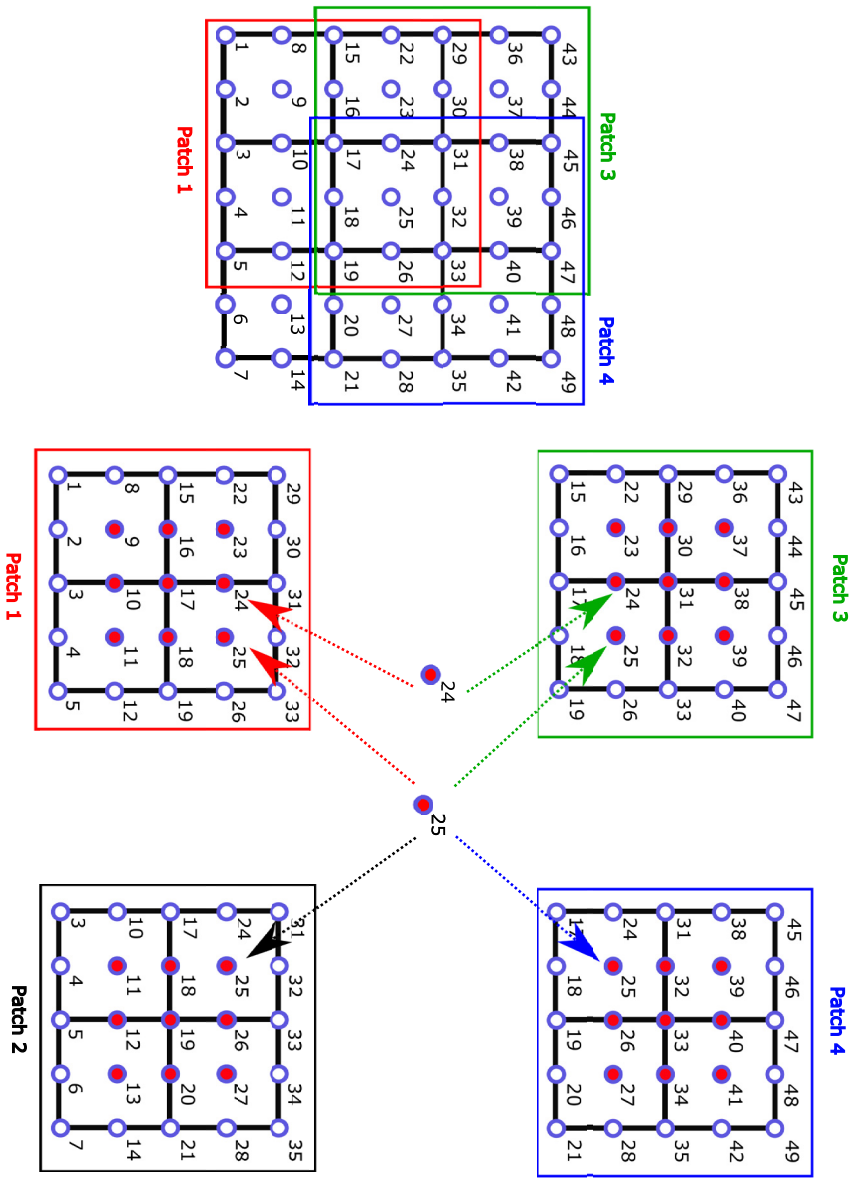

Fig. 4. Overlapping of patches.

$G_{12} = G_{13} = G_{23} = 0.37 \times 10^6$ psi (2.551 GPa), $\nu_{12} = 0.32$

- Material-IV: [18,29]
  $E_1 = 1.8282 \times 10^6$ psi (12.604 GPa), $E_2 = 1.8315 \times 10^6$ psi (12.627 GPa),
  $G_{12} = G_{13} = G_{23} = 3.125 \times 10^5$ psi (2.155 GPa), $\nu_{12} = 0.2395$
- Material-V: [63,76]
  Facesheet: $E_1 = 139$ GPa, $E_2 = 9.86$ GPa, $G_{12} = G_{13} = G_{23} = 5.24$ GPa, $\nu_{12} = 0.3$
  Core: $E_1 = E_2 = 0.09$ GPa, $G_{12} = G_{13} = G_{23} = 0.032$ GPa, $\nu_{12} = 0.45$

4.2. Boundary conditions

As the present formulation is based on displacement approach with C^0 continuity, so it is required to satisfy only kinematics boundary conditions, i.e., (u_0, v_0, w_0, ϕ_x, ϕ_y, θ_x, θ_y). The different types of boundary conditions, most commonly encounter in practice, are considered for present study of full geometrically nonlinear analysis of laminated and sandwich composite plates.

- Simply supported
  1. For cross-ply [57]
     SSSS1: $u_0 = w_0 = \theta_x = \phi_x = 0$ at $y = 0, b$ and $v_0 = w_0 = \theta_y = \phi_y = 0$ at $x = 0, a$
  2. For angle-ply [57]
     SSSS2: $v_0 = w_0 = \theta_x = \phi_x = 0$ at $y = 0, b$ and $u_0 = w_0 = \theta_y = \phi_y = 0$ at $x = 0, a$
  3. Immovable hard (Hinged) [18]
     SSSS3: $u_0 = v_0 = w_0 = \theta_x = \phi_x = 0$ at $y = 0, b$ and $u_0 = v_0 = w_0 = \theta_y = \phi_y = 0$ at $x = 0, a$

4. Immovable soft [18]
   SSSS4: $u_0 = v_0 = w_0 = 0$ at $y = 0, b$ and $x = 0, a$
- Clamped [57]
  CCCC: $u_0 = v_0 = w_0 = \theta_x = \theta_y = \phi_x = \phi_y = 0$ at $y = 0, b$ and $x = 0, a$
- SSFSX
  S at $y = 0$, S at $x = b$, no condition at $y = b$, S at $x = 0$
  Here,'X' signifies the type of simply supported, i.e., 1, 2, 3, or 4.

4.3. Numerical results and discussions

In all the following examples, unless specified otherwise, all layers are assumed to be equal in thickness, and all the present solutions are obtained at 12×12 mesh discretization. For the post-processing of stresses, the superconvergent patch recovery technique with 2×2 Legendre-Gauss sampling is used.

Linear analysis

In this part, the linear analysis has been carried out to validate the present formulation before going for the detailed nonlinear analysis. Moreover, to investigate the accuracy in a more authentic way, Navier type closed form solutions (CFSs) using IHSDT have been obtained, as there is an unavailability of the closed form solutions for some cases. These closed form solutions are then used to assess the accuracy of the FEM-IHSDT solution and to calibrate the value of the penalty parameter, γ. The mathematical formulation for the Navier type closed form solutions is shown in the Appendix B.

4.3.1. Simply supported symmetric cross-ply square laminated plate under SSL

In order to validate the present formulation, a simply supported ($SSSS1$) four layered $(0^0/90^0/90^0/0^0)$ square composite plate under sinusoidal distributed load (SSL), $P = P_0 sin(\pi x/a) sin(\pi y/b)$ is considered for investigation. The plate is made of $Material - I$ (given in Section 4.1). The normalized deflection and stresses computed by present FEM formulation are presented in Table 1 for different penalty parameter, γ. The normalized quantities used for comparison are:

$$\bar{w} = w_0\left(\frac{a}{2}, \frac{b}{2}\right)\left(\frac{100E_2h^3}{a^4P_0}\right) \quad \bar{\sigma}_{xx} = \sigma_{xx}\left(\frac{a}{2}, \frac{b}{2}, \frac{h}{2}\right)\left(\frac{h^2}{b^2P_0}\right)$$

$$\bar{\sigma}_{yy} = \sigma_{yy}\left(\frac{a}{2}, \frac{b}{2}, \frac{h}{4}\right)\left(\frac{h^2}{b^2P_0}\right) \quad \bar{\tau}_{xy} = \tau_{xy}\left(0, 0, \frac{h}{2}\right)\left(\frac{h^2}{b^2P_0}\right)$$

$$\bar{\tau}_{yz} = \tau_{yz}\left(\frac{a}{2}, 0, 0\right)\left(\frac{h}{bP_0}\right) \quad \bar{\sigma}_{yy} = \tau_{xz}\left(0, \frac{b}{2}, 0\right)\left(\frac{h}{bP_0}\right)$$

It can be observed from the Table 1 that the present solutions (for both TSDT and IHSDT using $\gamma = 10^7$) are found to be in good agreement with their respective Navier type closed form solutions (CFSs). The results also reveal that the effect of the penalty parameter is not much significant for the deflection characteristic of a symmetric cross-ply laminated plate. The relative change occurs in the deflection and stresses values without penalty constraints ($\gamma = 0$) is about 0.17% and 3.7%, respectively for IHSDT, and 0.45% and 5.7%, respectively for TSDT with respect to solutions using $\gamma = 10^7$. Particularly, IHSDT yields better solutions than TSDT at low span-to-thickness ratio ($a/h = 4$) as it is more close to 3D elasticity solution [69].

4.3.2. Simply supported anti-symmetric cross-ply square laminated plate under SSL

To the best of authors' knowledge, most of the studies available in the literature deal with the symmetric cross-ply laminated plate, although anti-symmetric cross-ply laminated plates are also important and possess important application. Therefore, to get a clear understanding of the accuracy of the present model, a comparison study has been carried out for anti-symmetric cross-ply laminated plate.

In this example, two $(0^0/90^0)$ and six $(0^0/90^0/0^0/90^0/0^0/90^0)$ layered anti-symmetric cross-ply laminated plates under $SSSS1$ boundary condition, subjected to sinusoidal distributed load (SSL), $P = P_0 sin(\pi x/a) sin(\pi y/b)$, are considered for investigation. The plate is made of $Material - I$ (listed in 4.1). In Table 2, present FEM solutions along with Navier type closed form solutions (CFSs) of TSDT and IHSDT are tabulated for the given plates with different a/h ratio. It is observed from the Table 2 that the effect of penalty parameter ($\gamma = 0$) is substantial for thick ($a/h = 4$) anti-symmetric cross-ply plate, i.e., 5.95% relative change in the deflection value with respect to $\gamma = 10^7$. The reason for this discrepancy can be attributed to the presence of extensional-bending coupling in the material stiffness matrix. Also, it is ascertained that as the number of layers increases the importance of penalty constraints decreases due to the vanishing of extensional-bending coupling. Hence, it is important to consider the penalty constraint in the formulation for the anti-symmetric cross-ply plate. In contrast to the previous example here, TSDT yields higher and more accurate results than IHSDT as the TSDT solutions are more close to the 3D elasticity solution of Zenkour [77] which emphasize the usage of TSDT for the anti-symmetric cross-ply plate to get the more accurate solution.

The above two linear examples clearly show that the incorporation of penalty stiffness is essential for the accurate analysis of the thick anti-symmetric laminated plate. Moreover, the effect of penalty constraints can be ignored in the thin plate. Apart from validating the present finite element formulation for linear bending analysis of laminated plate, linear results also highlight the usage of IHSDT for symmetric cross-ply laminated plates and TSDT for the anti-symmetric cross-ply plate to have a better solution. Moreover, it acknowledges the gap for further study to find an accurate NPSDT model for cross-ply plates, including an anti-symmetric cross-ply plate.

Nonlinear analysis

This section deals with the nonlinear bending analysis of isotropic and laminated composite plates. Unless specified otherwise, all the calculations are performed using a penalty parameter with value $\gamma = 10^7$, which yields sufficient accuracy as observed in the linear

Table 1
Normalized deflection and normalized stresses of simply supported ($SSSS1$) four layered $(0^0/90^0/90^0/0^0)$ square laminated plate under sinusoidal distributed load (SSL).

a/h	Source/Model	γ penalty	$\bar{w}$	$\bar{\sigma}_{xx}$	$\bar{\sigma}_{yy}$	$\bar{\tau}_{xy}$	$\bar{\tau}_{yz}$	$\bar{\tau}_{xz}$
			$\left(\frac{a}{2}, \frac{b}{2}, 0\right)$	$\left(\frac{a}{2}, \frac{b}{2}, \frac{h}{2}\right)$	$\left(\frac{a}{2}, \frac{b}{2}, \frac{h}{4}\right)$	$\left(0, 0, \frac{h}{2}\right)$	$\left(\frac{a}{2}, 0, 0\right)$	$\left(0, \frac{b}{2}, 0\right)$
4	3D Elasticity [69]		1.9540	0.7200	0.6630	0.0467	0.2920	0.2190
	CFS-IHSDT [5]	-	1.9257	0.7240	0.6396	0.0473	0.2699	0.2505
	CFS-TSDT [69]	-	1.8940	0.6650	0.6320	0.0440	0.2390	0.2060
	FEM-IHSDT†	10^7	1.9257	0.7254	0.6390	0.0473	0.2699	0.2504
	FEM-TSDT†	10^7	1.8937	0.6651	0.6322	0.0440	0.2390	0.2064
	FEM-IHSDT†	10^4	1.9258	0.7255	0.6390	0.0473	0.2700	0.2505
	FEM-TSDT†	10^4	1.8937	0.6651	0.6322	0.0441	0.2390	0.2065
	FEM-IHSDT†	0	1.9290	0.6994	0.6400	0.0468	0.2706	0.2445
	(relative change)		(0.17%)	(3.7%)	(0.15%)	(1%)	(0.25%)	(2.41%)
	FEM-TSDT†	0	1.9023	0.7057	0.6309	0.0461	0.2460	0.2138
	(relative change)		(0.45%)	(5.7%)	(0.2%)	(4.5%)	(2.8%)	(3.46%)
100	3D-Elasticity [69]		0.4380	0.5390	0.2760	0.0216	0.1410	0.3370
	CFS-IHSDT [5]	-	0.4344	0.5385	0.2710	0.0213	0.1269	0.3643
	CFS-TSDT [69]	-	0.4340	0.5390	0.2710	0.0213	0.1120	0.2900
	FEM-IHSDT†	10^7	0.4344	0.5387	0.2709	0.0213	0.1271	0.3643
	FEM-TSDT†	10^7	0.4343	0.5387	0.2708	0.0213	0.1117	0.2898
	FEM-IHSDT†	10^4	0.4345	0.5388	0.2709	0.0213	0.1271	0.3644
	FEM-TSDT†	10^4	0.4343	0.5387	0.2708	0.0213	0.1117	0.2899
	FEM-IHSDT†	0	0.4345	0.5389	0.2709	0.0213	0.1278	0.3724
	FEM-TSDT†	0	0.4344	0.5388	0.2708	0.0213	0.1153	0.3156

†Present results using C^0 finite element approach; CFS stands for closed form solution.

Table 2
Effect of penalty parameter, γ on normalized deflection, $\bar{w} = w_0\left(\frac{a}{2}, \frac{b}{2}\right)\left(\frac{100E_2h^3}{a^4P_0}\right)$ of simply supported ($SSSS1$) anti-symmetric cross-ply $\left(0^0/90^0\right)_n$ square laminated plate under sinusoidal distributed load (SSL).

Layers	Source/Model	γ penalty	a/h					
			4	5	10	20	50	100
2 ($n=1$)	CFS-IHSDT*	-	1.8898	1.6009	1.2009	1.0981	1.0691	1.0650
	CFS-TSDT [69]	-	1.9985	1.6670	1.2161	1.1018	1.0697	1.0651
	FEM-IHSDT†	10^7	1.8898	1.6009	1.2009	1.0981	1.0691	1.0649
	FEM-TSDT†	10^7	1.9985	1.6670	1.2161	1.1018	1.0697	1.0651
	FEM-IHSDT†	10^4	1.8898	1.6009	1.2009	1.0981	1.0691	1.0650
	FEM-TSDT†	10^4	1.9986	1.6670	1.2161	1.1018	1.0697	1.0651
	FEM-IHSDT†	0	2.0094	1.6704	1.2159	1.1017	1.0697	1.0651
	(relative change)		(5.95%)	(4.16%)	(1.23%)	(0.32%)	(0.05%)	(0.01%)
	FEM-TSDT†	0	2.0318	1.6852	1.2197	1.1.027	1.0698	1.0651
	(relative change)		(1.63%)	(1%)	(0.3%)	(0.08%)	(0.01%)	(0%)
4 ($n=2$)	3D-Elasticity [77]	-	1.9581	-	0.7624	0.5716	0.5170	0.5092
	CFS-IHSDT*	-	1.5909	1.2116	0.6866	0.5518	0.5137	0.5083
	CFS-TSDT*	-	1.6093	1.2184	0.6865	0.5517	0.5137	0.5083
6 ($n=3$)	CFS-IHSDT*	-	1.4932	1.1346	0.6344	0.5052	0.4687	0.4634
	CFS-TSDT [69]	-	1.5411	1.1590	0.6382	0.5060	0.4688	0.4635
	FEM-IHSDT†	10^7	1.4932	1.1346	0.6344	0.5052	0.4687	0.4634
	FEM-TSDT†	10^7	1.5411	1.1590	0.6382	0.5060	0.4688	0.4635
	FEM-IHSDT†	10^4	1.4932	1.1346	0.6344	0.5052	0.4687	0.4634
	FEM-TSDT†	10^4	1.5411	1.1590	0.6382	0.5060	0.4688	0.4635
	FEM-IHSDT†	0	1.5277	1.1509	0.6367	0.5057	0.4688	0.4635
	(relative change)		(2.25%)	(1.41%)	(0.36%)	(0.09%)	(0.02%)	(0.01%)
	FEM-TSDT†	0	1.5423	1.1591	0.6338	0.5060	0.4688	0.4635
	(relative change)		(0.07%)	(0.01%)	(0.69%)	(0%)	(0%)	(0%)
8 ($n=4$)	3D-Elasticity [77]	-	1.7903	-	0.6698	0.5037	0.4569	0.4504
	CFS-IHSDT*	-	1.4647	1.1118	0.6184	0.4908	0.4547	0.4496
	CFS-TSDT*	-	1.5168	1.1387	0.6228	0.4917	0.4549	0.4496

†Present results using C^0 finite element approach.
*Present results using Navier approach; CFS stands for closed form solution.

analysis. Both von Kármán and Green-Lagrange nonlinearities are taken to show a significant difference in the solutions, and accordingly, the utilization of the same for various plates under different boundary conditions has been suggested for a better solution. Apart from the nonlinearity, different deformation models have also been utilized for a wide range of problems to compare and suggests some measures to have better accuracy for the particular static problem. For validation and comparison purposes, ANSYS solutions are also obtained in MECHANICAL APDL 18.1 as solutions were not available for nonlinear bending analysis of plates with one free edge. In ANSYS, a 3D 4node 181 shell element is utilized. For discretization, 50×50 mesh has been used for plate subjected to sinusoidal distributed load (SSL), while 12×12 mesh has been considered for the uniformly distributed load (UDL) case.

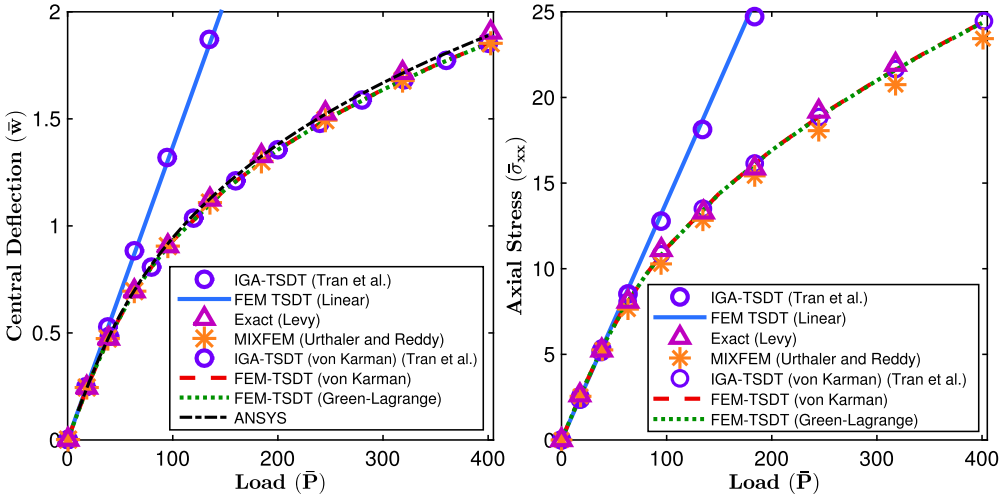

(a) Normalized central deflection ($\bar{w}$) vs load factor ($\bar{P}$). **(b)** Normalized axial stress ($\bar{\sigma}_{xx}$) vs load factor ($\bar{P}$).

Fig. 5. Comparison of normalized central deflection and normalized axial stress of thin isotropic clamped square plate subjected to uniformly distributed load (UDL).

4.3.3. Clamped thin square isotropic plate under uniformly distributed load

In this example, a thin ($a/h = 100$) square isotropic plate subjected to uniformly distributed load (UDL), $P = P_0$ with all sides fully constraints ($CCCC$) is considered for validation. The material constants for this isotropic plate are $E = 206.84$ GPa and $\nu = 0.316$. This problem has also been studied by many authors like Levy [78], Urthaler and Reddy [36], Tran et al. [18] for validation of geometrically nonlinear analysis. Fig. 5 shows nonlinear variation of normalized central deflection, $\bar{w} = w\left(\frac{a}{2}, \frac{b}{2}\right)/h$ and axial stress, $\bar{\sigma}_{xx} = \sigma_{xx}\left(\frac{a}{2}, \frac{b}{2}, \frac{h}{2}\right)a^2/E_2h^2$ versus load parameter, $\bar{P} = P_0a^4/E_2h^4$. Figs. 5a and 5b show that the obtained results using FEM-TSDT are in good agreement with those of double Fourier (exact) solution [78], FSDT based mixed finite element (MIXFEM) solution [36], and TSDT based isogeometric solution (IGA-TSDT) [18] with von Kármán nonlinearity. It is important to note that no difference is obtained between von Kármán and Green-Lagrange solutions of FEM-TSDT due to consideration of thin plate, $a/h = 100$. For the sake of brevity FEM-IHSDT solution is not shown as it exactly overlaps with FEM-TSDT solution. The ANSYS solution has also been obtained and found to be in well agreement with other solutions and the little discrepancies could be attributed to FSDT being used in the ANSYS package.

4.3.4. Isotropic plate subjected to UDL under different type of boundary conditions with one free edge

Here, an isotropic square plate with in-plane dimensions, $a = b = 10$ in, and thickness, $h = 1$ in, with material properties $E = 7.8 \times 10^6$ psi and $\nu = 0.3$ [55] is considered for the nonlinear bending analysis. The plate is subjected to uniformly distributed load (UDL) under different set of boundary conditions. The analysis is carried out under the consideration of von Kármán as well as Green-Lagrange sense of strain-displacement nonlinearity, and the obtained results are illustrated in Fig. 6. The normalized central deflections, $\bar{w} = w\left(\frac{a}{2}, \frac{b}{2}\right)/h$ for $CCCC$, $SSSS2$, and $SSSS4$ boundary condition are plotted against the load parameter, $\bar{P} = P_0a^4/Eh^4$ and found to be almost same in the both nonlinear strain-displacement relations. However, in the boundary conditions $CCFC$, $SSFS2$, $SSFS4$, a substantial difference is observed, which in turn ascertain the utility of Green-Lagrange strain nonlinearity in the nonlinear analysis. Also, the central deflections obtained using Green-Lagrange nonlinearity are found to be lower than the von Kármán results (see Fig. 6) due to more terms involved in the Green-Lagrange formulation. However, ANSYS results predict higher central deflection at large load parameter, $\bar{P}$. The reason for this discrepancy can be attributed to the formulation used in the ANSYS package, i.e., utilization of FSDT with thickness stretching and other parameters along with the imposition of boundary conditions. It is important to note that a significant difference is observed between von Kármán and Green-Lagrange results for $SSSS1$ and $SSFS1$ due to the contribution of normal in-plane displacement in the nonlinear strain. This difference emphasizes the use of Green-Lagrange strain relation for plates with one free edge. The same emphasis is provided by the closeness of Green-Lagrange FEM results and ANSYS results. As per authors' knowledge, this type of novel results with their validation is not found in the literature and can be considered benchmark results for future investigation using Green-Lagrange nonlinearity.

4.3.5. Orthotropic and four-layered square laminated plates under UDL

Particularly, this set of problems is considered as the benchmark problem for the validation of the laminated composite plate. In the first part, a simply supported ($SSSS1$) square orthotropic plate with material properties $Material - III$ [18,29], under uniformly distributed load (UDL), is considered. The plate dimensions are $a = b = 12$ in and $h = 0.138$ in. In second part, a four-layered $(0^0/90^0/90^0/0^0)$ square laminated plate under uniformly distributed load (UDL) with material properties $Material - IV$ is studied with $a = b = 12$ in and $h = 0.096$ in. Fig. 7 reveals that the present FEM results are found to be well-matched with IGA-TSDT results of Tran et al. [18] which validate our formulation for the laminated composite plate. However, in the clamped plate (in Fig. 7b), there is a discrepancy between experimental [29] and present FEM results. This may be attributed to inadequate clamped boundary constraints in the experimental setup and uncertainty in the material properties of the specimen. Moreover, the importance of shear deformation for orthotropic material is vindicated in this problem by the large discrepancy possessed by the finite-difference results of CPT [29].

4.3.6. Hinged symmetric laminated plate under UDL

In this example, a four layered $(0^0/90^0/90^0/0^0)$ square composite plate with all sides hinged ($SSSS3$), subjected to uniformly distributed load (UDL), is considered. Each layer of the plate is made of $Material - I$ [55]. For comparison the normalized central deflection,

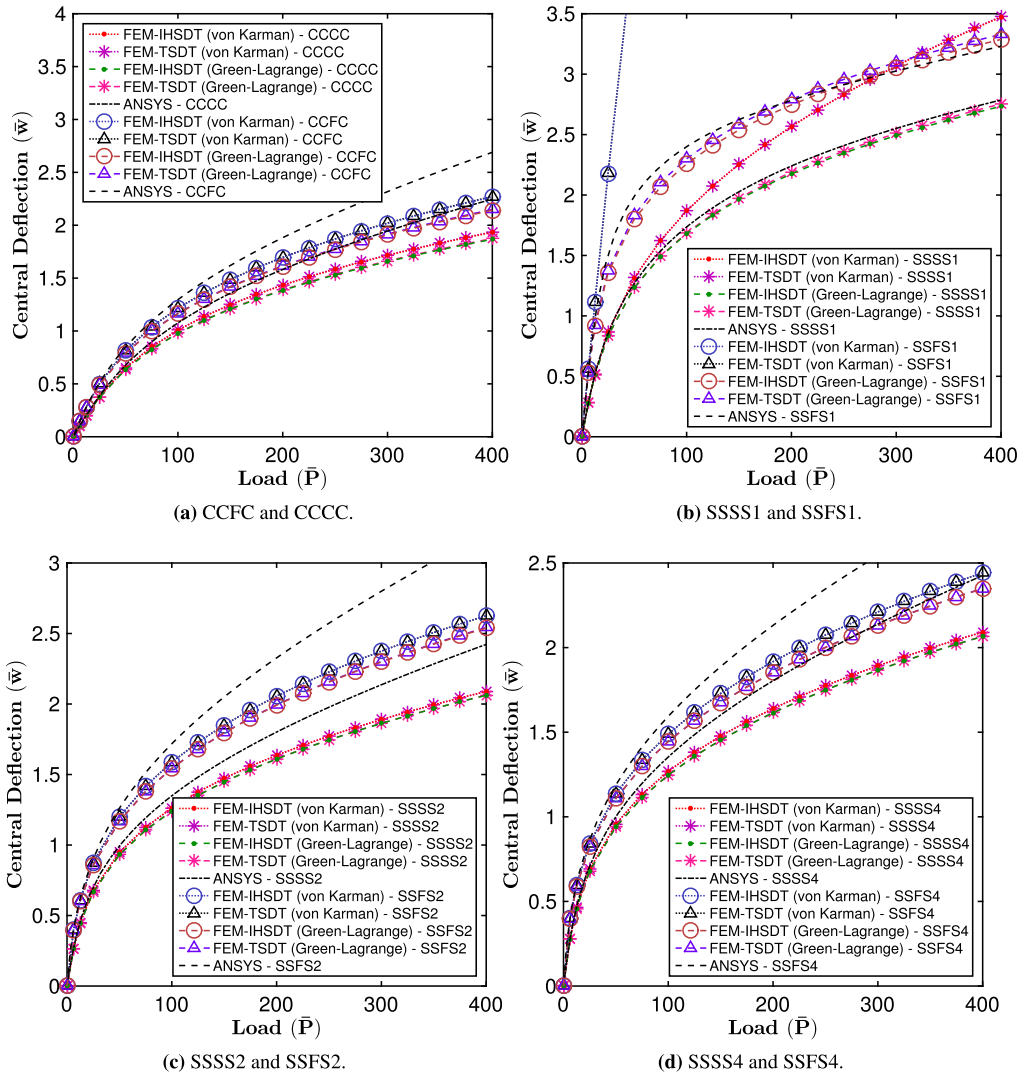

(a) CCFC and CCCC. **(b)** SSSS1 and SSFS1.

(c) SSSS2 and SSFS2. **(d)** SSSS4 and SSFS4.

Fig. 6. Load-deflection curves of square isotropic plate subjected to uniformly distributed load (UDL) under different set of boundary conditions with $a/h = 10$.

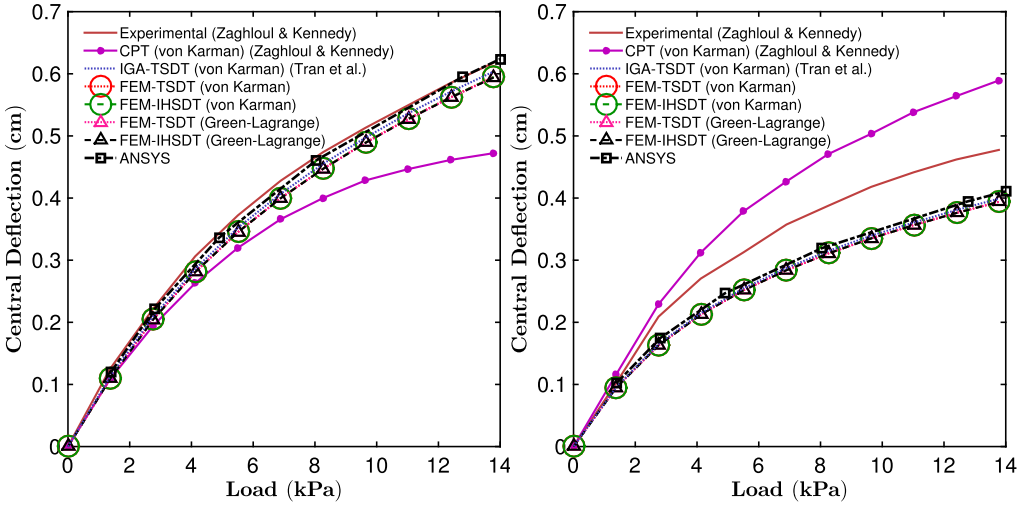

(a) Simply supported orthotropic plate. **(b)** Clamped laminated plate.

Fig. 7. Load-deflection curve of (a) simply supported square orthotropic plate (b) clamped square laminated $(0^0/90^0/90^0/0^0)$ plate under uniformly distributed load (UDL).

Table 3
Normalized central deflection, $\bar{w}$ of simply supported ($SSSS3$) square laminated $(0^0/90^0/90^0/0^0)$ plate subjected to uniformly distributed load (UDL).

a/h	$\bar{P}$	C^0 HSDT* [79]	MISQ20* [80]	RDKQ-NL24* [35]	MQRBF* [51]	IGA-TSDT* [18]	FEM-TSDT* (Present)	FEM-TSDT† (Present)	FEM-IHSDT* (Present)	FEM-IHSDT† (Present)	ANSYS (Present)
40	50	0.293	0.296	0.294	0.2654	0.2936	0.2936	0.2935	0.2940	0.2939	0.2944
	100	0.464	0.473	0.467	0.446	0.4643	0.4643	0.4640	0.4647	0.4643	0.4649
	150	0.582	0.592	0.587	0.616	0.5798	0.5798	0.5973	0.5801	0.5796	0.5803
	200	0.664	0.683	0.679	0.7355	0.6683	0.6682	0.6675	0.6685	0.6678	0.6687
	250	0.738	0.759	0.754	0.8355	0.7407	0.7408	0.7400	0.7410	0.7402	0.7414
20	50	0.320	0.312	0.327	0.3004	0.3126	0.3126	0.3120	0.3139	0.3133	0.3149
	100	0.493	0.487	0.494	0.5085	0.4807	0.4807	0.4793	0.4818	0.4804	0.4823
	150	0.592	0.603	0.608	0.6591	0.5928	0.5928	0.5909	0.5937	0.5918	0.5942
	200	0.680	0.691	0.695	0.7780	0.6784	0.6784	0.6760	0.6791	0.6768	0.6797
	250	0.752	0.765	0.766	0.8771	0.7486	0.7486	0.7459	0.7492	0.7465	0.7500
10	50	0.360	0.356	0.370	-	0.3609	0.3601	0.3587	0.3634	0.3613	0.3647
	100	0.520	0.521	0.525	-	0.5179	0.5170	0.5141	0.5199	0.5162	0.5206
	150	0.624	0.629	0.629	-	0.6213	0.6206	0.6163	0.6229	0.6181	0.6239
	200	0.696	0.711	0.710	-	0.7005	0.6994	0.6947	0.7019	0.6963	0.7040
	250	0.760	0.779	0.777	-	0.7659	0.7647	0.7594	0.7672	0.7608	0.7697

*Present results using von Kármán nonlinearity; †present results using Green-Lagrange nonlinearity.

Table 4
Normalized central deflection, $\bar{w}$ of simply supported ($SSSS1$) square laminated $(0^0/90^0/90^0/0^0)$ plate subjected to sinusoidal distributed load (SSL).

a/h	$\bar{P}$	FSDT# [18]	IGA-TSDT [18]	FEM-TSDT* (Present)	FEM-TSDT† (Present)	FEM-IHSDT* (Present)	FEM-IHSDT† (Present)	ANSYS (Present)
4	50	0.6791	0.7198	0.7197	0.6929	0.7265	0.7015	0.6867
	100	1.0788	1.1214	1.1217	1.0165	1.1261	1.0210	0.9522
	200	1.6111	1.6555	1.6555	1.3216	1.6512	1.3175	1.1860
	300	1.9877	2.0447	2.0387	1.4769	2.0283	1.4691	1.3042
10	50	0.3236	0.3474	0.3474	0.3462	0.3535	0.3525	0.3624
	100	0.6121	0.6501	0.6501	0.6433	0.6597	0.6536	0.6615
	200	1.0667	1.1148	1.1147	1.0866	1.1264	1.1002	1.1012
	300	1.4100	1.4612	1.4605	1.4033	1.4726	1.4176	1.4076
20	50	0.2428	0.2504	0.2508	0.2507	0.2528	0.2527	0.2543
	100	0.4734	0.4872	0.4872	0.4859	0.4907	0.4896	0.4963
	200	0.8763	0.8960	0.8960	0.8893	0.9012	0.8951	0.7084
	300	1.2024	1.2255	1.2250	1.2104	1.2308	1.2171	1.2232
100	50	0.2150	0.2159	0.2159	0.2159	0.2160	0.2160	0.2160
	100	0.4226	0.4243	0.4243	0.4243	0.4245	0.4244	0.4253
	200	0.7967	0.7993	0.7987	0.7985	0.7990	0.7988	0.7986
	300	1.1117	1.1146	1.1142	1.1137	1.1145	1.1140	1.1139

*Present results using von Kármán nonlinearity; †present results using Green-Lagrange nonlinearity.
#FSDT results using MITC element [81].

$\bar{w} = w_0\left(\frac{a}{2}, \frac{b}{2}\right)/h$ and normalized load parameter, $\bar{P} = P_0 a^4/E_2 h^4$ are considered. The present FEM and ANSYS results are compared with those available PSDT [18,79,80] and NPSDT [51] solutions and tabulated in Table 3. It can be observed from the Table 3 that the present von Kármán results are matching very well with the FE solution of Kant [79] and isogeometric results of Tran et al. [18] for $a/h = 10, 20, 40$. Moreover, a slightly lower deflection, around (1%), is obtained using Green-Lagrange nonlinearity at higher load parameter for moderately thick, $a/h = 10$ plate with respect to von Kármán results due to more nonlinear terms in the strain-displacement relation. It is to be noted that due to the restraint of in-plane (normal) displacements no significant difference is found between von Kármán and Green-Lagrange results.

4.3.7. Simply supported symmetric cross-ply laminated plate under SSL

The problem described in the previous Section 4.3.6 is again analyzed with simply supported boundary condition ($SSSS1$) and sinusoidal distributed load (SSL), $P = P_0 sin(\pi x/a) sin(\pi y/b)$, for different span-to-thickness ratios, $a/h = 4, 10, 20, 100$; and the obtained normalized central deflections, $\bar{w} = w\left(\frac{a}{2}, \frac{b}{2}\right)/h$ are tabulated in Table 4. The results show that a close agreement is found between IGA-TSDT solutions of Tran et al. [18] and present FEM-TSDT solutions as both utilize von Kármán sense of nonlinearity in their formulation. Note that, in comparison to the hinged constraint ($SSSS3$) (shown in the previous example), the effect of Green-Lagrange is more prominent in $SSSS1$. The reason for this discrepancy can be attributed to the unconstrained normal in-plane displacement in the $SSSS1$ boundary condition. It can be observed from the Table 4 that for the plate with $a/h = 4$, the relative difference between von Kármán results and Green-Lagrange results increases from 3% to 27% with increase in load parameter, from $\bar{P} = 50$ to $\bar{P} = 300$. Here, the relative difference is calculated with respect to von Kármán results. Note that a good agreement is found between Green-Lagrange results and ANSYS results which emphasizes the use of Green-Lagrange nonlinearity for movable simply supported plate ($SSSS1$).

For span-to-thickness ratio, $a/h = 10$, the through-thickness variation of normalized stresses for same problem, under sinusoidal distributed load (SSL), is illustrated in Fig. 8. As expected, at higher load, $\bar{P}$ nonlinearity due to strain-displacement is dominated, i.e., for the same normalized external load, lower normalized stresses are developed. It is important to emphasize that as load increases, asymmetry in the through-thickness distribution dominates in the in-plane stresses, $\bar{\sigma}_{xx}$, $\bar{\sigma}_{yy}$, and $\bar{\tau}_{xy}$, but symmetry retains in the transverse shear stresses, $\bar{\tau}_{yz}$ and $\bar{\tau}_{xz}$ as same has been observed by Tran et al. [18]. Further, an asymmetry is observed in the through-thickness variation of in-plane stresses due to Green-Lagrange nonlinearity. Moreover, the traction free boundary condition, which should

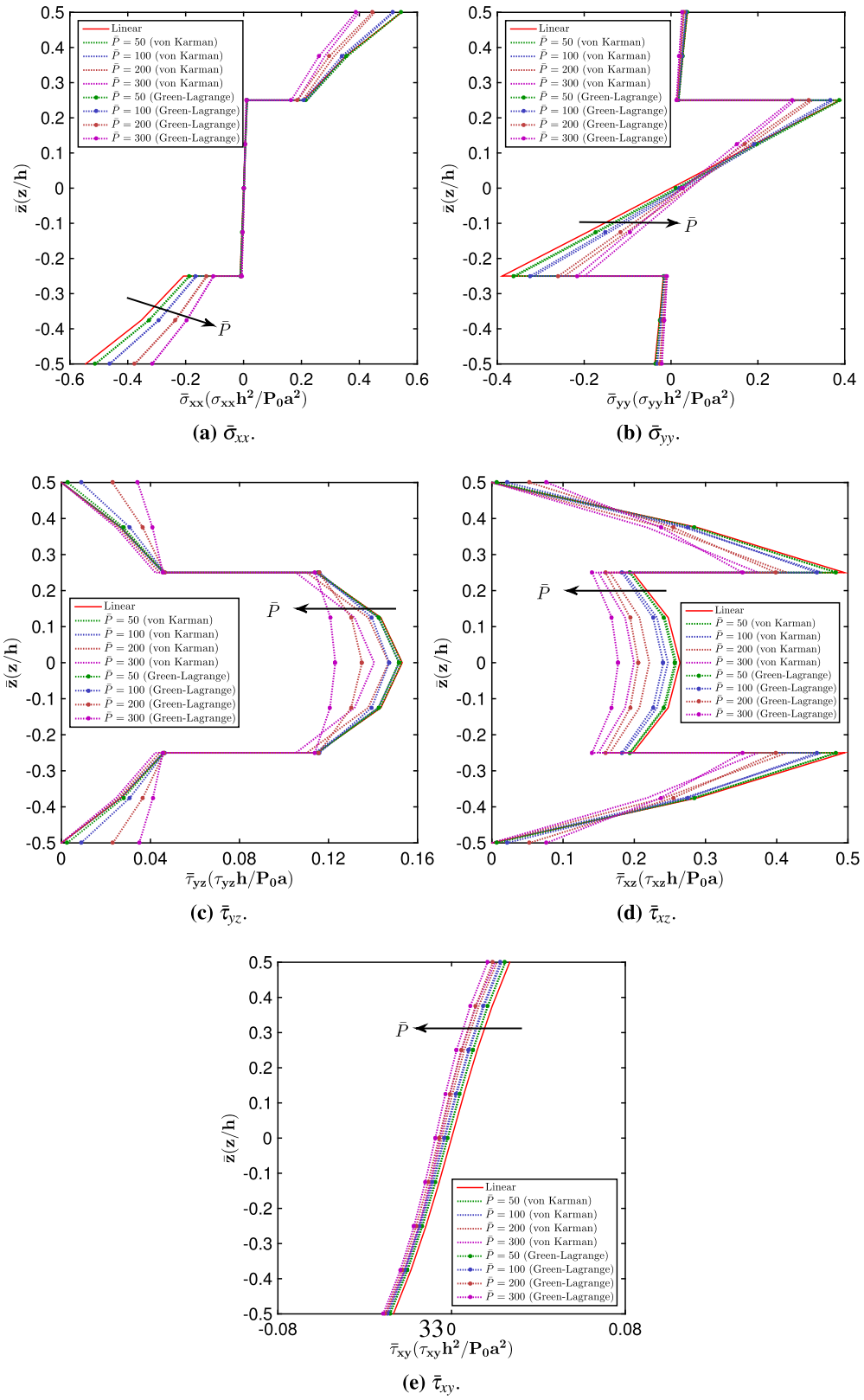

(a) $\bar{\sigma}_{xx}$. **(b)** $\bar{\sigma}_{yy}$.

(c) $\bar{\tau}_{yz}$. **(d)** $\bar{\tau}_{xz}$.

(e) $\bar{\tau}_{xy}$.

Fig. 8. Effect of increasing load parameter $\bar{P}$ on through thickness distribution of stresses of simply supported ($SSSS1$) square laminated $(0^0/90^0/90^0/0^0)$ plate subjected to sinusoidal distributed load (SSL) with $a/h = 10$: the curves corresponding to load parameters, $\bar{P} = 50$, 100, 200, and 300 are represented in green, blue, brown, and purple, respectively.

Table 5
Effect of penalty parameter on normalized central deflection, $\bar{w}$ of simply supported ($SSSS1$) anti-symmetric cross-ply $\left(0^0/90^0\right)_n$ laminated plate subjected to sinusoidal distributed load (SSL).

n	a/h	$\bar{P}$	FEM-TSDT*		FEM-TSDT†		FEM-IHSDT*		FEM-IHSDT†		ANSYS (Present)
			$\gamma = 10^7$	$\gamma = 0$	$\gamma = 10^7$	$\gamma = 0$	$\gamma = 10^7$	$\gamma = 0$	$\gamma = 10^7$	$\gamma = 0$	
1	4	50	0.5808	0.5883	0.5606	0.5655	0.5594	0.5845	0.5450	0.5621	0.6231
		100	0.9484	0.9582	0.8703	0.8780	0.9241	0.9542	0.8589	0.8751	0.8959
		200	1.4306	1.4499	1.2242	1.2481	1.4004	1.4457	1.2157	1.2500	1.1547
		300	1.7776	1.8112	1.4052	1.4585	1.7397	1.8067	1.3920	1.4564	1.2974
	100	50	0.3759	0.3759	0.3759	0.3758	0.3758	0.3758	0.3758	0.3758	0.3822
		100	0.6877	0.6877	0.6876	0.6876	0.6876	0.6877	0.6875	0.6875	0.6857
		200	1.1382	1.1382	1.1378	1.1378	1.1381	1.1381	1.1377	1.1378	1.1355
		300	1.4581	1.4581	1.4574	1.4575	1.4580	1.4581	1.4574	1.4575	1.4580
3	4	50	0.4554	0.4555	0.4498	0.4503	0.4450	0.4521	0.4418	0.4470	0.4638
		100	0.7922	0.7926	0.7627	0.7670	0.7788	0.7882	0.7571	0.7874	0.7336
		200	1.2603	1.2647	1.1644	1.1660	1.2419	1.2595	1.1374	1.1654	1.0109
		300	1.6038	1.6167	1.3391	1.3502	1.5786	1.6108	1.3429	1.3578	1.1546
	100	50	0.1511	0.1511	0.1511	0.1511	0.1511	0.1511	0.1511	0.1511	0.1505
		100	0.2999	0.2999	0.2999	0.2999	0.2999	0.2999	0.2999	0.2999	0.2989
		200	0.5832	0.5832	0.5831	0.5831	0.5832	0.5832	0.5831	0.5831	0.5818
		300	0.8412	0.8411	0.8409	0.8409	0.8411	0.8411	0.8409	0.8409	0.8389

*Present results using von Kármán nonlinearity; †present results using Green-Lagrange nonlinearity.

be satisfied in 3D equilibrium, is satisfied only in linear and von Kármán nonlinearity cases. The reason for this is the assumed traction free condition initially imposed in linear strain tensor which retains in von Kármán strain-displacement relation and constitutive approach used for obtaining the transverse stresses. Whereas, due to the contribution of extra terms in the nonlinear transverse strain components, this traction free boundary condition is relaxed in the Green-Lagrange results. Thus, the traction free boundary condition imposed during linear analysis remains valid in von Kármán nonlinearity but not in Green-Lagrange nonlinearity. It is to be noted that no stress recovery technique is used in thickness direction and transverse stresses are obtained through constitutive relation which leads to non-zero traction condition. Hence, it is recommended that the use of constitutive relation for transverse stresses should be limited to linear and von Kármán nonlinearity. While, a 3D equilibrium approach [72,73,75] must be used in thickness direction while considering the Green-Lagrange non-linearity. As per authors' knowledge, this types of observations have not been reported in the available literature.

4.3.8. Effect of penalty parameter on nonlinear bending response of anti-symmetric cross-ply square plate under SSL

In this example, the effect of the penalty parameter, γ on the geometrically nonlinear bending analysis incorporating both von Kármán and Green-Lagrange sense of nonlinearity is investigated. To demonstrate this, a simply supported ($SSSS1$) anti-symmetric cross-ply square laminated plate subjected to sinusoidal distributed load (SSL) is considered with each ply made of $Material-II$ [69]. Table 5 shows that as load increases the effect of penalty becomes significant in thick plate, $a/h = 4$, in comparison to thin plate, $a/h = 100$. For instance, the relative difference due to the effect of penalty parameter for $\left(0^0/90^0\right)$ plate is found to be around 1.9% for von Kármán TSDT, 3.8% Green-Lagrange TSDT, 3.8% for von Kármán IHSDT, and 4.6% for Green-Lagrange IHSDT with respect to solutions at $\gamma = 10^7$ for $\bar{P} = 300$. It is to be noticed that in this example a material with higher orthotropic nature is considered i.e., $E_1/E_2 = 40$ in comparison to previous problems where $E_1/E_2 = 25$. Moreover, this relative difference increases with the load parameter, $\bar{P}$. Thus, the effect of penalty stiffness is important for those plates which possess strong extensional-bending coupling and decreases as the number of layers increases. Similar to the linear analysis of anti-symmetric cross-ply, here also, the performance of TSDT is found to be marginally better than IHSDT. Note that a good agreement is found between Green-Lagrange results and ANSYS results. However, a little discrepancy is found, which can be due to the formulation used in the ANSYS package, i.e., FSDT with thickness stretching effect, and convergence and tolerance parameter utilized in it.

4.3.9. Laminated composite plate subjected to UDL under different boundary conditions with one free edge

In this example, a laminated composite plate with one free edge subjected to uniformly distributed load (UDL) is considered for nonlinear analysis. The other three edges are subjected to a different set of boundary conditions. For this study, a square laminated plate ($a = b = 10$ in) having material properties $Material-I$ [55] with $E_2 = 10^6$ psi is taken for parametric study. In Fig. 9a the effect of different boundary conditions $SSSS1$ and $SSFS1$ for thick, $a/h = 4$ and thin, $a/h = 50$ for symmetric four-layered $\left(0^0/90^0/90^0/0^0\right)$ laminated composite plate is illustrated. It is observed that in the case of all simply supported ($SSSS1$) edges, von Kármán and Green-Lagrange solutions agree quite well for $a/h = 50$. However, in the case of a $SSFS1$ boundary condition distinguishable response is observed due to the significant contribution of Green-Lagrange strain term with an increase in the value of load parameter, $\bar{P} = P_0 a^4/E_2 h^4$. Moreover, the difference increases (with respect to normalized load parameter, $\bar{P}$) as the plate becomes thicker. Fig. 9b emphasizes that as the number of layers increases, the discrepancy between von Kármán and Green-Lagrange results, for $SSFS1$ boundary condition, decreases due to the vanishing of bending-extensional coupling. Fig. 9c shows that, in comparison with $\left(45^0/-45^0\right)_2$, a large discrepancy between von Kármán and Green-Lagrange results is found with $\left(0^0/90^0\right)_2$ lamination. The reason for this discrepancy can be attributed to high magnitude of bending-extension coupling possesses by anti-symmetric cross-ply lamination with lower bending stiffness matrix. Note that, in all different cases, ANSYS results are also plotted, which shows a reasonably good agreement with Green-Lagrange results and highlights the importance of Green-Lagrange nonlinearity over von Kármán nonlinearity.

4.3.10. Simply supported anti-symmetric cross-ply and angle-ply laminated plates under UDL

In this example, a simply supported ($SSSS1$) square laminated plate with $Material-II$ [69], under uniformly distributed load (UDL), is considered for parametric study. The results are obtained to assess the influence of the number of layers on the nonlinear bending

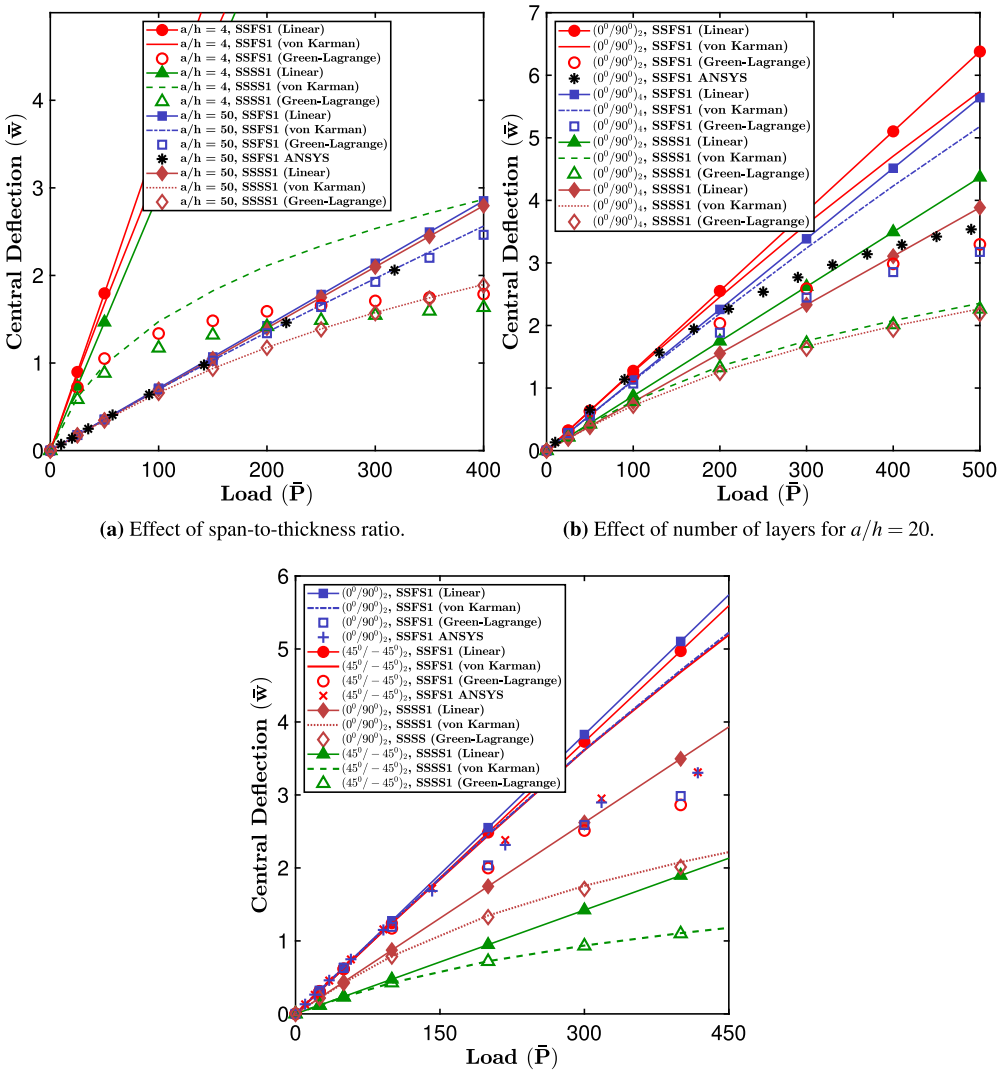

(a) Effect of span-to-thickness ratio.

(b) Effect of number of layers for $a/h = 20$.

(c) Effect of fiber orientation for $a/h = 20$.

Fig. 9. Effect of span-to-thickness ratio, number of layers, and fiber orientation on load-deflection curve of square laminated plate with one free edge subjected to uniformly distributed load (UDL).

response of plate with $a/h = 4$ and 10, and the same is shown in Fig. 10. It can be observed from the Fig. 10 that as the number of layers increases, the effect of nonlinearity decreases as depicted from the difference between linear and nonlinear results. Moreover, the effect of nonlinearity is more prominent in a thick plate, $a/h = 4$. Furthermore, a small difference is observed between von Kármán and Green-Lagrange nonlinearity for the moderately thick plate, $a/h = 10$.

In Fig. 11, the effect of the fiber orientation on the bending response of anti-symmetric angle-ply $(-\theta/\theta/-\theta/\theta)$ plate is shown. Here, it can be observed that the difference between linear and nonlinear is constant for various anti-symmetric angle-ply plates for $a/h = 10$. This difference implies that as the fiber angle increases, only bending characteristic increases, leading to lower the central deflection. Moreover, the effect of nonlinearity is prominent in thick plates, $a/h = 4$, i.e., a significant difference is observed between linear and nonlinear characteristics of plate with $a/h = 10$.

In Fig. 12, the variation of normalized central deflection with fiber orientation of symmetric and anti-symmetric angle-ply composite plate is illustrated. It is found that fiber with 45^0 orientation is optimal for design, and anti-symmetric angle-ply possesses marginally more bending stiffness than the symmetric angle-ply plate. It is to be noted that here in this set of examples, the $SSSS1$ boundary condition is considered.

4.3.11. Five-layered simply supported square sandwich plate under UDL

To demonstrate the applicability of the present C^0 finite element model for sandwich plates, a five-layered square sandwich plate is considered in this example for nonlinear bending analysis. The plate is composed of five layers of $Material - V$ [63,76], where the top and the bottom two layers are of equal thickness. The top/bottom two layers form the face-sheet with thickness, h_f, and the middle layer with thickness, h_c forms the core of the sandwich. The geometrically nonlinear bending behavior of the simply supported ($SSSS4$) five-layered $\left(0^0/90^0/C/90^0/0^0\right)$ square sandwich plate is analyzed using the IHSDT model, and the same is compared with FEM solution of normal deformation theory by Madhukar and Singha [63]. The equilibrium path of normalized central deflection, $\bar{w} = w\left(\frac{a}{2}, \frac{b}{2}\right)/h$ and normalized load parameter, $\bar{P} = P_0 a^4/E_2 h^4$ is obtained for different a/h ratios and h_c/h_f ratios, and the same is shown in Figs. 13 and 14,

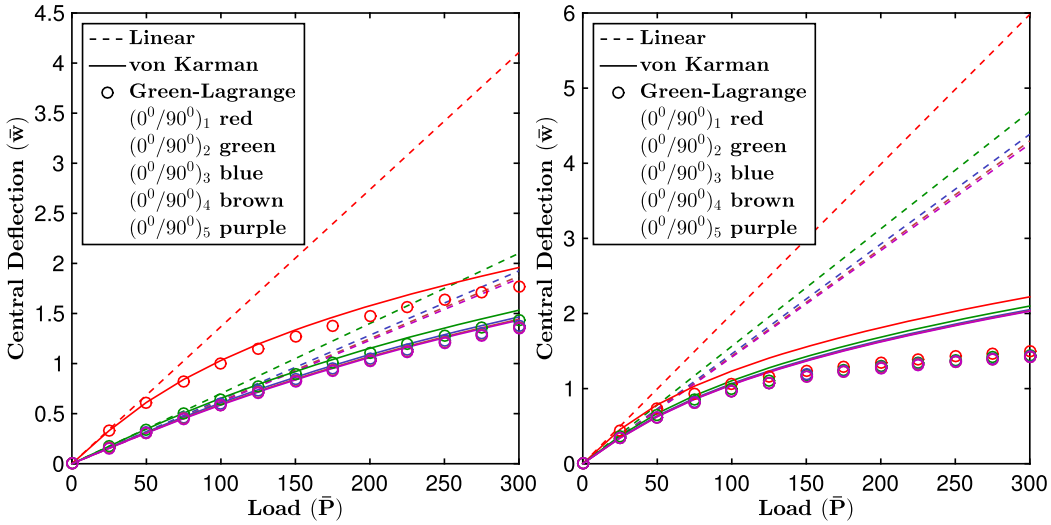

(a) $a/h = 10$. **(b)** $a/h = 4$.

Fig. 10. Effect of number of layers on load-deflection curve of simply supported ($SSSS1$) cross-ply $\left(0^0/90^0\right)_n$ laminated plate subjected to uniformly distributed load (UDL) with $a/h = 10$ and $a/h = 4$.

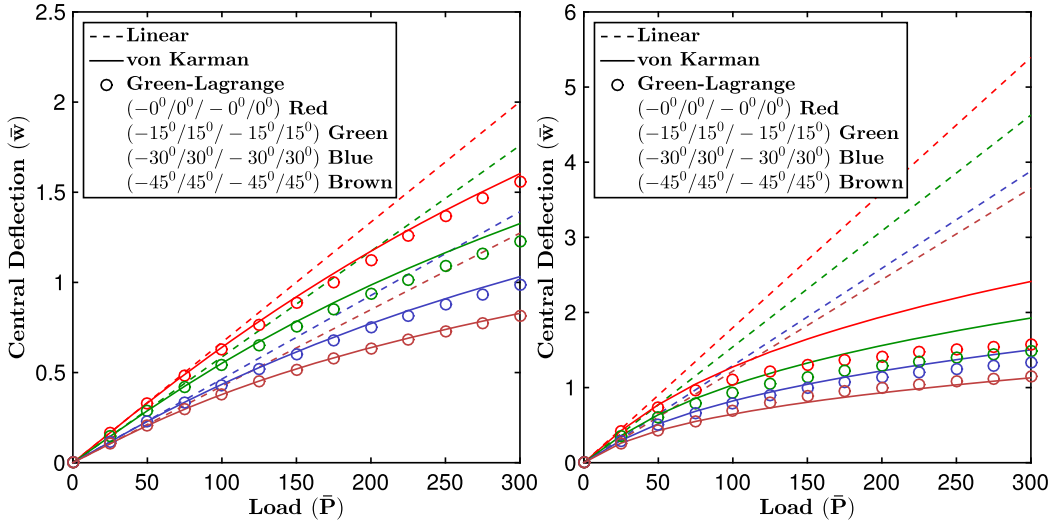

(a) $a/h = 10$. **(b)** $a/h = 4$.

Fig. 11. Effect of fiber orientation on load-deflection curves of simply supported ($SSSS1$) anti-symmetric angle-ply $(-\theta/\theta/-\theta/\theta)$ laminated plate subjected to uniformly distributed load (UDL) with $a/h = 10$ and $a/h = 4$.

respectively; where E_2 is the material constant of face-sheet. The Figs. 13 and 14 show that a close agreement is found between present FEM-IHSDT solution and Madhukar and Singha solution [63], which validates the applicability of the present finite element model for sandwich plates.

5. Conclusion

In this paper, the importance of Green-Lagrange nonlinearity over von Kármán nonlinearity is highlighted via means of employing a C^0 finite element plate model for linear and nonlinear bending analysis using higher-order shear deformation theories (HSDTs). The importance of penalty consideration is also emphasized as it is revealed that this plays a crucial role in securing a more accurate solution in some cases.

A nine-noded C^0 finite element model with the consideration of penalty constraints is formulated for the bending analysis of isotropic, laminated, and sandwich plates. The study emphatically reveals several facts and insights regarding the need for full geometric nonlinearity, usage of the penalty parameter, and the superiority of deformation theories. It is found that the neglect of the penalty parameter in the formulation leads to substantial error in both linear and nonlinear analysis, and to get the accurate response, the value of the penalty parameter should be of the order of material constants. Further, the importance of Green-Lagrange strain relation in the formulation is highlighted through various examples, and it is observed that the consideration of full geometric nonlinearity becomes essential for the boundary conditions with a free edge or with movable simply supported boundary condition ($SSSS1$). Besides, the effect of full geometric nonlinearity and the effect of the penalty parameter are found to be prominent in thick plates with $a/h \leq 10$. Further, it was found that

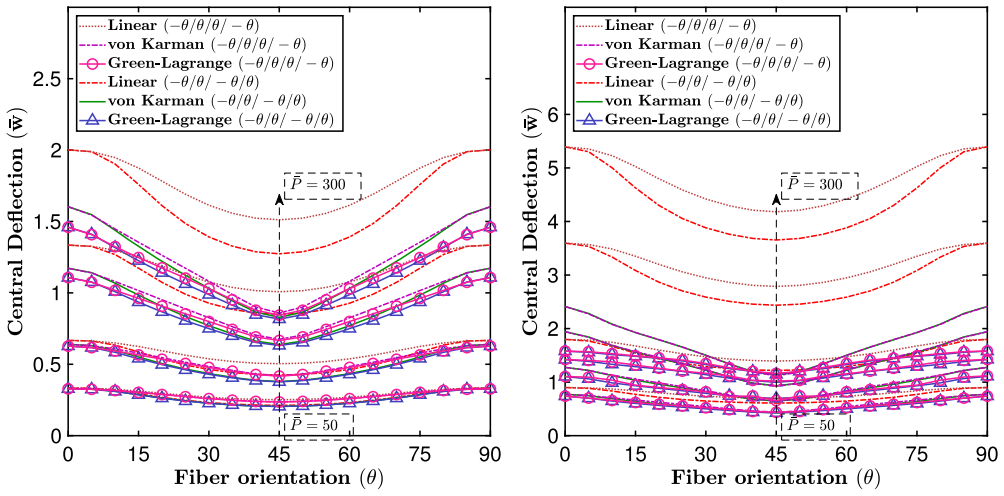

(a) $a/h = 10$. **(b)** $a/h = 4$.

Fig. 12. Effect of fiber orientation on nonlinear bending response of symmetric and anti-symmetric angle-ply laminated plates subjected to uniformly distributed load (UDL) with $a/h = 10$ and $a/h = 4$.

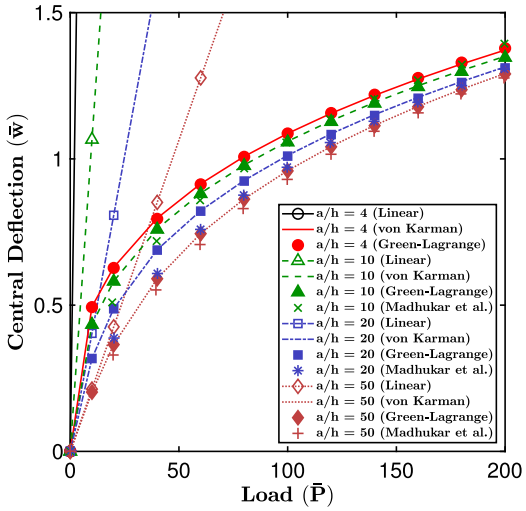

Fig. 13. Effect of span-to-thickness ratio, a/h on nonlinear bending response of simply supported $(SSSS4)$ square sandwich $(0^0/90^0/C/90^0/0^0)$ plate under uniformly distributed load (UDL) with $h_c/h_f = 5$.

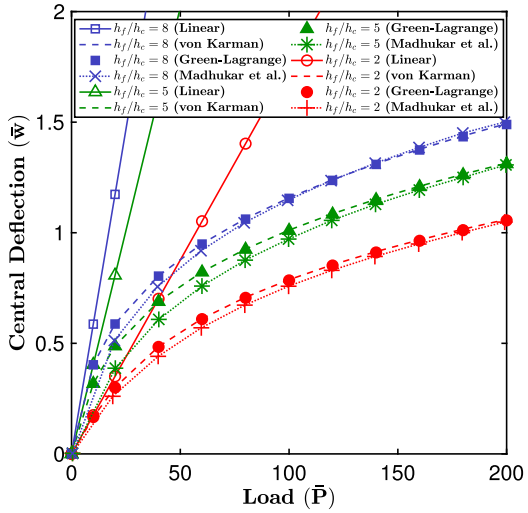

Fig. 14. Effect of core-to-facesheet thickness ratio, h_c/h_f on nonlinear bending response of simply supported $(SSSS4)$ square sandwich $(0^0/90^0/C/90^0/0^0)$ plate under uniformly distributed load (UDL) with $a/h = 20$.

the traction free boundary conditions on the top and bottom surfaces of the plate are only satisfied in linear and von Kármán nonlinear analysis, but not in the Green-Lagrange nonlinear analysis when obtained from constitutive approach. Moreover, for the moderately thick plate, $a/h = 10$, the through-thickness variation of in-plane stresses is found to be unsymmetrical. Thus, to accurately calculate the transverse stresses for the Green-Lagrange nonlinearity, a stress recovery technique employing the equilibrium approach must be considered for traction free boundary conditions.

In addition, the performance of polynomial and nonpolynomial shear deformation theories (PSDT & NPSDT) is holistically studied for various structural parameters under the consideration of full geometric nonlinearity. Moreover, a comparative study is carried out for various parameters such as lamination schemes, side-to-thickness ratios, and others. In case of bending analysis, the IHSDT is found to be performing better for the symmetric cross-ply, whereas the TSDT is found to be performing better for the anti-symmetric cross-ply multilayered composite plates. The work presented in this paper provides a strong background to delve into the wide scope of the NPSDT for the further study of structural analysis.

Declaration of competing interest

The authors declare that they have no known competing financial interests or personal relationships that could have appeared to influence the work reported in this paper.

Appendix A. The expression of $\mathbb{N}_b$ and $\mathbb{N}_s$

$$\mathbb{N}_b = \begin{bmatrix}
N_{xx} & N_{xy} & 0 & 0 & 0 & 0 & M_{xx} & M_{xy} & 0 & 0 & P_{xx} & P_{xy} & 0 & 0 \\
N_{xy} & N_{yy} & 0 & 0 & 0 & 0 & M_{xy} & M_{yy} & 0 & 0 & P_{xy} & P_{yy} & 0 & 0 \\
0 & 0 & N_{xx} & N_{xy} & 0 & 0 & 0 & 0 & M_{xx} & M_{xy} & 0 & 0 & P_{xx} & P_{xy} \\
0 & 0 & N_{xy} & N_{yy} & 0 & 0 & 0 & 0 & M_{xy} & M_{yy} & 0 & 0 & P_{xy} & P_{yy} \\
0 & 0 & 0 & 0 & N_{xx} & N_{xy} & 0 & 0 & 0 & 0 & 0 & 0 & 0 & 0 \\
0 & 0 & 0 & 0 & N_{xy} & N_{yy} & 0 & 0 & 0 & 0 & 0 & 0 & 0 & 0 \\
M_{xx} & M_{xy} & 0 & 0 & 0 & 0 & Q_{xx} & Q_{xy} & 0 & 0 & R_{xx} & R_{xy} & 0 & 0 \\
M_{xy} & M_{yy} & 0 & 0 & 0 & 0 & Q_{xy} & Q_{yy} & 0 & 0 & R_{xy} & R_{yy} & 0 & 0 \\
0 & 0 & M_{xx} & M_{xy} & 0 & 0 & 0 & 0 & Q_{xx} & Q_{xy} & 0 & 0 & R_{xx} & R_{xy} \\
0 & 0 & M_{xy} & M_{yy} & 0 & 0 & 0 & 0 & Q_{xy} & Q_{yy} & 0 & 0 & R_{xy} & R_{yy} \\
P_{xx} & P_{xy} & 0 & 0 & 0 & 0 & R_{xx} & R_{xy} & 0 & 0 & S_{xx} & S_{xy} & 0 & 0 \\
P_{xy} & P_{yy} & 0 & 0 & 0 & 0 & R_{xy} & R_{yy} & 0 & 0 & S_{xy} & S_{yy} & 0 & 0 \\
0 & 0 & 0 & 0 & 0 & 0 & 0 & 0 & R_{xx} & R_{xy} & 0 & 0 & S_{xx} & S_{xy} \\
0 & 0 & 0 & 0 & 0 & 0 & 0 & 0 & R_{xy} & R_{yy} & 0 & 0 & S_{xy} & S_{yy}
\end{bmatrix}$$

$$\mathbb{N}_s = \begin{bmatrix}
0 & 0 & 0 & 0 & N_{xz} & N_{yz} & 0 & 0 & M_{xz} & M_{yz} & 0 & 0 & P_{xz} & P_{yz} & 0 & 0 \\
0 & 0 & 0 & 0 & 0 & 0 & N_{xz} & N_{yz} & 0 & 0 & M_{xz} & M_{yz} & 0 & 0 & P_{xz} & P_{yz} \\
0 & 0 & 0 & 0 & Q_{xz} & Q_{yz} & 0 & 0 & R_{xz} & R_{yz} & 0 & 0 & S_{xz} & S_{yz} & 0 & 0 \\
0 & 0 & 0 & 0 & 0 & 0 & Q_{xz} & Q_{yz} & 0 & 0 & R_{xz} & R_{yz} & 0 & 0 & S_{xz} & S_{yz} \\
N_{xz} & 0 & Q_{xz} & 0 & 0 & 0 & 0 & 0 & 0 & 0 & 0 & 0 & 0 & 0 & 0 & 0 \\
N_{yz} & 0 & Q_{yz} & 0 & 0 & 0 & 0 & 0 & 0 & 0 & 0 & 0 & 0 & 0 & 0 & 0 \\
0 & N_{xz} & 0 & Q_{xz} & 0 & 0 & 0 & 0 & 0 & 0 & 0 & 0 & 0 & 0 & 0 & 0 \\
0 & N_{yz} & 0 & Q_{yz} & 0 & 0 & 0 & 0 & 0 & 0 & 0 & 0 & 0 & 0 & 0 & 0 \\
M_{xz} & 0 & R_{xz} & 0 & 0 & 0 & 0 & 0 & 0 & 0 & 0 & 0 & 0 & 0 & 0 & 0 \\
M_{yz} & 0 & R_{yz} & 0 & 0 & 0 & 0 & 0 & 0 & 0 & 0 & 0 & 0 & 0 & 0 & 0 \\
0 & M_{xz} & 0 & R_{xz} & 0 & 0 & 0 & 0 & 0 & 0 & 0 & 0 & 0 & 0 & 0 & 0 \\
0 & M_{yz} & 0 & R_{yz} & 0 & 0 & 0 & 0 & 0 & 0 & 0 & 0 & 0 & 0 & 0 & 0 \\
P_{xz} & 0 & S_{xz} & 0 & 0 & 0 & 0 & 0 & 0 & 0 & 0 & 0 & 0 & 0 & 0 & 0 \\
P_{yz} & 0 & S_{yz} & 0 & 0 & 0 & 0 & 0 & 0 & 0 & 0 & 0 & 0 & 0 & 0 & 0 \\
0 & P_{xz} & 0 & S_{xz} & 0 & 0 & 0 & 0 & 0 & 0 & 0 & 0 & 0 & 0 & 0 & 0 \\
0 & P_{yz} & 0 & S_{yz} & 0 & 0 & 0 & 0 & 0 & 0 & 0 & 0 & 0 & 0 & 0 & 0
\end{bmatrix}$$

Appendix B. Navier solution for simply supported ($SSSS1$) anti-symmetric cross-ply composite plate

$$u_0 = \sum_{m=1}^{\infty}\sum_{n=1}^{\infty} U_{mn} cos\,(\alpha x)\, sin\,(\beta y) \qquad v_0 = \sum_{m=1}^{\infty}\sum_{n=1}^{\infty} V_{mn} sin\,(\alpha x)\, cos\,(\beta y)$$

$$w_0 = \sum_{m=1}^{\infty}\sum_{n=1}^{\infty} W_{mn} sin\,(\alpha x)\, sin\,(\beta y) \qquad \theta_x = \sum_{m=1}^{\infty}\sum_{n=1}^{\infty} X_{mn} cos\,(\alpha x)\, sin\,(\beta y)$$

$$\theta_y = \sum_{m=1}^{\infty}\sum_{n=1}^{\infty} Y_{mn} sin\,(\alpha x)\, cos\,(\beta y)$$

$$\begin{bmatrix} K_{11} & K_{12} & K_{13} & K_{14} & K_{15} \\ & K_{22} & K_{23} & K_{24} & K_{25} \\ & & K_{33} & K_{34} & K_{35} \\ & \text{sym} & & K_{44} & K_{45} \\ & & & & K_{55} \end{bmatrix} \begin{Bmatrix} U_{mn} \\ V_{mn} \\ W_{mn} \\ X_{mn} \\ Y_{mn} \end{Bmatrix} = \begin{Bmatrix} 0 \\ 0 \\ F_{mn} \\ 0 \\ 0 \end{Bmatrix}$$

$$\begin{aligned}
K_{11} &= \alpha^2 A_{11} + \beta^2 A_{66} \\
K_{12} &= \alpha\beta A_{12} + \alpha\beta A_{66} \\
K_{13} &= -\alpha\left(\alpha^2 B_{11} + \beta^2 B_{12} + 2\beta^2 B_{66}\right) \\
K_{14} &= \alpha^2 C_{11} + \beta^2 C_{66} \\
K_{15} &= \alpha\beta C_{12} + \alpha\beta C_{66} \\
K_{22} &= \alpha^2 A_{66} + \beta^2 A_{22} \\
K_{23} &= -\beta\left(\alpha^2 B_{12} + \beta^2 B_{22} + 2\alpha^2 B_{66}\right) \\
K_{24} &= \alpha\beta C_{12} + \alpha\beta C_{66} \\
K_{25} &= \alpha^2 C_{66} + \beta^2 C_{22} \\
K_{33} &= \alpha^4 D_{11} + 2\alpha^2\beta^2 D_{12} + \beta^4 D_{22} + 4\alpha^2\beta^2 D_{66} \\
K_{34} &= -\alpha\left(\alpha^2 E_{11} + \beta^2 E_{12} + 2\beta^2 E_{66}\right) \\
K_{35} &= -\beta\left(\alpha^2 E_{12} + \beta^2 E_{22} + 2\alpha^2 E_{66}\right) \\
K_{44} &= A_{55} + \alpha^2 F_{11} + \beta^2 F_{66} \\
K_{45} &= \alpha\beta F_{12} + \alpha\beta F_{66} \\
K_{55} &= A_{44} + \alpha^2 F_{66} + \beta^2 F_{22}
\end{aligned}$$

;

$$\begin{aligned}
[A_{ij}] &= \int_{-h/2}^{h/2} \bar{Q}_{ij} dz \\
[B_{ij}] &= \int_{-h/2}^{h/2} z\bar{Q}_{ij} dz \\
[C_{ij}] &= \int_{-h/2}^{h/2} f(z)\, \bar{Q}_{ij} dz \\
[D_{ij}] &= \int_{-h/2}^{h/2} G(z)\, \bar{Q}_{ij} dz \\
[E_{ij}] &= \int_{-h/2}^{h/2} z^2 \bar{Q}_{ij} dz \qquad ; \\
[F_{ij}] &= \int_{-h/2}^{h/2} z f(z)\, \bar{Q}_{ij} dz \\
i, j &= \quad 1, 2, 6 \\
[A_{ij}] &= \int_{-h/2}^{h/2} f'(z)\, \bar{Q}_{ij} dz \\
i, j &= \quad 4, 5
\end{aligned}$$

$$F_{mn} = \begin{cases} P_0 & \text{Sinusoidal distributed load (SSL)} \\ 16P_0/\pi^2 mn & \text{Uniformly distributed load (UDL)} \end{cases}$$

References

[1] B.R. Thakur, S. Verma, B. Singh, D. Maiti, Dynamic analysis of folded laminated composite plate using nonpolynomial shear deformation theory, Aerosp. Sci. Technol. 106 (2020) 106083, https://doi.org/10.1016/j.ast.2020.106083.

[2] A. Gupta, A. Ghosh, Isogeometric static and dynamic analysis of laminated and sandwich composite plates using nonpolynomial shear deformation theory, Composites, Part B, Eng. 176 (2019) 107295, https://doi.org/10.1016/j.compositesb.2019.107295.

[3] A.S. Sayyad, Y.M. Ghugal, On the free vibration analysis of laminated composite and sandwich plates: a review of recent literature with some numerical results, Compos. Struct. 129 (2015) 177–201, https://doi.org/10.1016/j.compstruct.2015.04.007.

[4] S. Abrate, M.D. Sciuva, Equivalent single layer theories for composite and sandwich structures: a review, Compos. Struct. 179 (2017) 482–494, https://doi.org/10.1016/j.compstruct.2017.07.090.

[5] N. Grover, D. Maiti, B. Singh, A new inverse hyperbolic shear deformation theory for static and buckling analysis of laminated composite and sandwich plates, Compos. Struct. 95 (2013) 667–675, https://doi.org/10.1016/j.compstruct.2012.08.012.

[6] T.N. Nguyen, C.H. Thai, H. Nguyen-Xuan, On the general framework of high order shear deformation theories for laminated composite plate structures, A novel unified approach, Int. J. Mech. Sci. 110 (2016) 242–255, https://doi.org/10.1016/j.ijmecsci.2016.01.012.

[7] D.B. Singh, B.N. Singh, Assessment and accuracy of new nonpolynomial shear deformation theories for static analysis of laminated and braided composite plates, J. Aerosp. Eng. 30 (5) (2017) 04017056, https://doi.org/10.1061/(asce)as.1943-5525.0000768.

[8] A. Lal, N.J. Kanu, The nonlinear deflection response of CNT/nanoclay reinforced polymer hybrid composite plate under different loading conditions, IOP Conf. Ser., Mater. Sci. Eng. (2020) 814, https://doi.org/10.1088/1757-899x/814/1/012033, 012033.

[9] J. Mantari, C.G. Soares, Optimized sinusoidal higher order shear deformation theory for the analysis of functionally graded plates and shells, Composites, Part B, Eng. 56 (2014) 126–136, https://doi.org/10.1016/j.compositesb.2013.07.027.

[10] J. Mantari, E. Bonilla, C.G. Soares, A new tangential-exponential higher order shear deformation theory for advanced composite plates, Composites, Part B, Eng. 60 (2014) 319–328, https://doi.org/10.1016/j.compositesb.2013.12.001.

[11] J. Yarasca, J. Mantari, M. Petrolo, E. Carrera, Best theory diagrams for cross-ply composite plates using polynomial, trigonometric and exponential thickness expansions, Compos. Struct. 161 (2017) 362–383, https://doi.org/10.1016/j.compstruct.2016.11.053.

[12] J.L. Mantari, J. Yarasca, M. Petrolo, E. Carrera, On the effects of trigonometric and exponential terms on the best theory diagrams for metallic, multilayered, and functionally graded plates, Mech. Adv. Mat. Struct. 27 (5) (2018) 426–440, https://doi.org/10.1080/15376494.2018.1478048.

[13] J. Monge, J. Mantari, S. Charca, N. Vladimir, An axiomatic/asymptotic evaluation of the best theories for free vibration of laminated and sandwich shells using non-polynomial functions, Eng. Struct. 172 (2018) 1011–1024, https://doi.org/10.1016/j.engstruct.2018.06.020.

[14] J. Monge, J. Mantari, Best non-polynomial shear deformation theories for cross-ply single skin and sandwich shells, Eng. Struct. 203 (2020) 109678, https://doi.org/10.1016/j.engstruct.2019.109678.
[15] B.R. Thakur, S. Verma, B. Singh, D. Maiti, Geometrically nonlinear dynamic analysis of laminated composite plate using a nonpolynomial shear deformation theory, Int. J. Non-Linear Mech. 128 (2021) 103635, https://doi.org/10.1016/j.ijnonlinmec.2020.103635.
[16] I. Shufrin, O. Rabinovitch, M. Eisenberger, A semi-analytical approach for the geometrically nonlinear analysis of trapezoidal plates, Int. J. Mech. Sci. 52 (12) (2010) 1588–1596, https://doi.org/10.1016/j.ijmecsci.2010.07.008.
[17] P. Dash, B.N. Singh, Static response of geometrically nonlinear laminated composite plates having uncertain material properties, Mech. Adv. Mat. Struct. 22 (4) (2014) 269–280, https://doi.org/10.1080/15376494.2012.736056.
[18] L.V. Tran, J. Lee, H. Nguyen-Van, H. Nguyen-Xuan, M.A. Wahab, Geometrically nonlinear isogeometric analysis of laminated composite plates based on higher-order shear deformation theory, Int. J. Non-Linear Mech. 72 (2015) 42–52, https://doi.org/10.1016/j.ijnonlinmec.2015.02.007.
[19] P. Phung-Van, T. Nguyen-Thoi, T. Bui-Xuan, Q. Lieu-Xuan, A cell-based smoothed three-node Mindlin plate element (CS-FEM-MIN3) based on the c0-type higher-order shear deformation for geometrically nonlinear analysis of laminated composite plates, Comput. Mater. Sci. 96 (2015) 549–558, https://doi.org/10.1016/j.commatsci.2014.04.043.
[20] R. Ansari, R. Hassani, R. Gholami, H. Rouhi, Nonlinear bending analysis of arbitrary-shaped porous nanocomposite plates using a novel numerical approach, Int. J. Non-Linear Mech. 126 (2020) 103556, https://doi.org/10.1016/j.ijnonlinmec.2020.103556.
[21] M.A. Bennaceur, Y. Xu, Application of the natural element method for the analysis of composite laminated plates, Aerosp. Sci. Technol. 87 (2019) 244–253, https://doi.org/10.1016/j.ast.2019.02.038.
[22] H. Fukunaga, N. Hu, G. Ren, FEM modeling of adaptive composite structures using a reduced higher-order plate theory via penalty functions, Int. J. Solids Struct. 38 (48–49) (2001) 8735–8752, https://doi.org/10.1016/s0020-7683(01)00072-5.
[23] A. Lal, N.M. Kulkarni, V.H. Siddaramaiah, Stochastic hygro-thermo-mechanically induced nonlinear static analysis of piezoelectric elastically support sandwich plate using secant function based shear deformation theory (SFSDT), Int. J. Comput. Mater. Sci. Eng. 05 (04) (2016) 1650020, https://doi.org/10.1142/s2047684116500202.
[24] B. Adhikari, B. Singh, An efficient higher order non-polynomial quasi 3-d theory for dynamic responses of laminated composite plates, Compos. Struct. 189 (2018) 386–397, https://doi.org/10.1016/j.compstruct.2017.10.044.
[25] R. Kumar, A. Lal, B.M. Sutaria, Non-linear deflection and stress analysis of laminated composite sandwich plate with elliptical cutout under different transverse loadings in hygro-thermal environment, Curv. Layered Struct. 7 (1) (2020) 80–100, https://doi.org/10.1515/cls-2020-0008.
[26] M.H. Kishore, B. Singh, M. Pandit, Nonlinear static analysis of smart laminated composite plate, Aerosp. Sci. Technol. 15 (3) (2011) 224–235, https://doi.org/10.1016/j.ast.2011.01.003.
[27] N. Tsushima, T. Yokozeki, W. Su, H. Arizono, Geometrically nonlinear static aeroelastic analysis of composite morphing wing with corrugated structures, Aerosp. Sci. Technol. 88 (2019) 244–257, https://doi.org/10.1016/j.ast.2019.03.025.
[28] M. Javani, Y. Kiani, M. Eslami, Geometrically nonlinear rapid surface heating of temperature-dependent FGM arches, Aerosp. Sci. Technol. 90 (2019) 264–274, https://doi.org/10.1016/j.ast.2019.04.049.
[29] S.A. Zaghloul, J.B. Kennedy, Nonlinear behavior of symmetrically laminated plates, J. Appl. Mech. 42 (1) (1975) 234–236, https://doi.org/10.1115/1.3423532.
[30] D.D. Milašinović, Geometric non-linear analysis of thin plate structures using the harmonic coupled finite strip method, Thin-Walled Struct. 49 (2) (2011) 280–290, https://doi.org/10.1016/j.tws.2010.11.005.
[31] M. Ren, J. Cong, B. Wang, L. Wang, Extended multiscale finite element method for large deflection analysis of thin-walled composite structures with complicated microstructure characteristics, Thin-Walled Struct. 130 (2018) 273–285, https://doi.org/10.1016/j.tws.2018.05.021.
[32] K.K. Shukla, Y. Nath, Nonlinear analysis of moderately thick laminated rectangular plates, J. Eng. Mech. 126 (8) (2000) 831–838, https://doi.org/10.1061/(asce)0733-9399(2000)126:8(831).
[33] K. Liew, J. Wang, M. Tan, S. Rajendran, Nonlinear analysis of laminated composite plates using the mesh-free kp-Ritz method based on FSDT, Comput. Methods Appl. Mech. Eng. 193 (45–47) (2004) 4763–4779, https://doi.org/10.1016/j.cma.2004.03.013.
[34] Y. Zhang, K. Kim, A simple displacement-based 3-node triangular element for linear and geometrically nonlinear analysis of laminated composite plates, Comput. Methods Appl. Mech. Eng. 194 (45–47) (2005) 4607–4632, https://doi.org/10.1016/j.cma.2004.11.011.
[35] Y. Zhang, K. Kim, Geometrically nonlinear analysis of laminated composite plates by two new displacement-based quadrilateral plate elements, Compos. Struct. 72 (3) (2006) 301–310, https://doi.org/10.1016/j.compstruct.2005.01.001.
[36] Y. Urthaler, J.N. Reddy, A mixed finite element for the nonlinear bending analysis of laminated composite plates based on FSDT, Mech. Adv. Mat. Struct. 15 (5) (2008) 335–354, https://doi.org/10.1080/15376490802045671.
[37] G. Rama, D. Marinkovic, M. Zehn, High performance 3-node shell element for linear and geometrically nonlinear analysis of composite laminates, Composites, Part B, Eng. 151 (2018) 118–126, https://doi.org/10.1016/j.compositesb.2018.06.007.
[38] S. Lim, K. Lee, S. Chow, N. Senthilnathan, Linear and nonlinear bending of shear-deformable plates, Comput. Struct. 30 (4) (1988) 945–952, https://doi.org/10.1016/0045-7949(88)90132-0.
[39] G. Singh, G. Rao, N. Iyengar, Geometrically nonlinear flexural response characteristics of shear deformable unsymmetrically laminated plates, Comput. Struct. 53 (1) (1994) 69–81, https://doi.org/10.1016/0045-7949(94)90131-7.
[40] M.C. Trinh, S.E. Kim, A three variable refined shear deformation theory for porous functionally graded doubly curved shell analysis, Aerosp. Sci. Technol. 94 (2019) 105356, https://doi.org/10.1016/j.ast.2019.105356.
[41] N. Putcha, J. Reddy, A refined mixed shear flexible finite element for the nonlinear analysis of laminated plates, Comput. Struct. 22 (4) (1986) 529–538, https://doi.org/10.1016/0045-7949(86)90002-7.
[42] J.K. Lim, Mixed-type finite element formulation of higher order shear deformation theory for the linear and nonlinear analyses of a laminated composite plate, KSME J. 4 (2) (1990) 109–114, https://doi.org/10.1007/bf02954031.
[43] D.G. Zhang, H.M. Zhou, Nonlinear bending analysis of FGM circular plates based on physical neutral surface and higher-order shear deformation theory, Aerosp. Sci. Technol. 41 (2015) 90–98, https://doi.org/10.1016/j.ast.2014.12.016.
[44] C.K. Hirwani, S.K. Panda, B.K. Patle, Theoretical and experimental validation of nonlinear deflection and stress responses of an internally debonded layer structure using different higher-order theories, Acta Mech. 229 (8) (2018) 3453–3473, https://doi.org/10.1007/s00707-018-2173-8.
[45] P.M. Vuong, N.D. Duc, Nonlinear response and buckling analysis of eccentrically stiffened FGM toroidal shell segments in thermal environment, Aerosp. Sci. Technol. 79 (2018) 383–398, https://doi.org/10.1016/j.ast.2018.05.058.
[46] S. Ghannadpour, N. Abdollahzadeh, Progressive failure analysis of thick imperfect composite plates using nonlinear plate theory, Int. J. Non-Linear Mech. 121 (2020) 103292, https://doi.org/10.1016/j.ijnonlinmec.2019.103292.
[47] L.V. Tran, S.E. Kim, Static and free vibration analyses of multilayered plates by a higher-order shear and normal deformation theory and isogeometric analysis, Thin-Walled Struct. 130 (2018) 622–640, https://doi.org/10.1016/j.tws.2018.06.013.
[48] Q. Cheng, T. Lok, Z.C. Xie, Geometrically non-linear analysis including shear deformation of composite laminates, Thin-Walled Struct. 35 (1) (1999) 41–59, https://doi.org/10.1016/s0263-8231(99)00016-6.
[49] M. Ćetković, Đ. Vuksanović, Geometrically nonlinear analysis of laminated composite plates using a layer wise displacement model, J. Serb. Soc. Computat. Mech. 5 (1) (2011) 50–68.
[50] F. Dau, O. Polit, M. Touratier, C1 plate and shell finite elements for geometrically nonlinear analysis of multilayered structures, Comput. Struct. 84 (19–20) (2006) 1264–1274, https://doi.org/10.1016/j.compstruc.2006.01.031.
[51] J. Singh, K. Shukla, Nonlinear flexural analysis of laminated composite plates using RBF based meshless method, Compos. Struct. 94 (5) (2012) 1714–1720, https://doi.org/10.1016/j.compstruct.2012.01.001.
[52] R. Kumar, A. Lal, B. Singh, J. Singh, Non-linear analysis of porous elastically supported FGM plate under various loading, Compos. Struct. 233 (2020) 111721, https://doi.org/10.1016/j.compstruct.2019.111721.
[53] H. Zafarmand, M. Kadkhodayan, Nonlinear material and geometric analysis of thick functionally graded plates with nonlinear strain hardening using nonlinear finite element method, Aerosp. Sci. Technol. 92 (2019) 930–944, https://doi.org/10.1016/j.ast.2019.07.015.

[54] G. Singh, Y.S. Rao, Large deflection behaviour of thick composite plates, Compos. Struct. 8 (1) (1987) 13–29, https://doi.org/10.1016/0263-8223(87)90013-4.
[55] T. Le-Manh, T. Luu-Anh, J. Lee, Isogeometric analysis for flexural behavior of composite plates considering large deformation with small rotations, Mech. Adv. Mat. Struct. 23 (3) (2015) 328–336, https://doi.org/10.1080/15376494.2014.981616.
[56] S.S. Sahoo, S.K. Panda, V.K. Singh, T.R. Mahapatra, Numerical investigation on the nonlinear flexural behaviour of wrapped glass/epoxy laminated composite panel and experimental validation, Arch. Appl. Mech. 87 (2) (2016) 315–333, https://doi.org/10.1007/s00419-016-1195-8.
[57] P. Dash, B. Singh, Geometrically nonlinear bending analysis of laminated composite plate, Commun. Nonlinear Sci. Numer. Simul. 15 (10) (2010) 3170–3181, https://doi.org/10.1016/j.cnsns.2009.11.017.
[58] M. Talha, B.N. Singh, Nonlinear mechanical bending of functionally graded material plates under transverse loads with various boundary conditions, Int. J. Model. Simul. Sci. Comput. 02 (02) (2011) 237–258, https://doi.org/10.1142/s1793962311000451.
[59] F. Alijani, M. Amabili, Non-linear static bending and forced vibrations of rectangular plates retaining non-linearities in rotations and thickness deformation, Int. J. Non-Linear Mech. 67 (2014) 394–404, https://doi.org/10.1016/j.ijnonlinmec.2014.10.003.
[60] B. Wu, A. Pagani, M. Filippi, W. Chen, E. Carrera, Large-deflection and post-buckling analyses of isotropic rectangular plates by Carrera unified formulation, Int. J. Non-Linear Mech. 116 (2019) 18–31, https://doi.org/10.1016/j.ijnonlinmec.2019.05.004.
[61] A. Pagani, E. Daneshkhah, X. Xu, E. Carrera, Evaluation of geometrically nonlinear terms in the large-deflection and post-buckling analysis of isotropic rectangular plates, Int. J. Non-Linear Mech. 121 (2020) 103461, https://doi.org/10.1016/j.ijnonlinmec.2020.103461.
[62] D. Elmalich, O. Rabinovitch, Geometrically nonlinear behavior of sandwich plates, AIAA J. 51 (8) (2013) 1993–2008, https://doi.org/10.2514/1.j052247.
[63] S. Madhukar, M. Singha, Geometrically nonlinear finite element analysis of sandwich plates using normal deformation theory, Compos. Struct. 97 (2013) 84–90, https://doi.org/10.1016/j.compstruct.2012.10.034.
[64] Y. Liang, B. Izzuddin, Large displacement analysis of sandwich plates and shells with symmetric/asymmetric lamination, Comput. Struct. 166 (2016) 11–32, https://doi.org/10.1016/j.compstruc.2016.01.001.
[65] L.T. That-Hoang, H. Nguyen-Van, T. Chau-Dinh, C. Huynh-Van, Enhancement to four-node quadrilateral plate elements by using cell-based smoothed strains and higher-order shear deformation theory for nonlinear analysis of composite structures, J. Sandw. Struct. Mater. (2018) 109963621879798, https://doi.org/10.1177/1099636218797982.
[66] P.V. Katariya, C.K. Hirwani, S.K. Panda, Geometrically nonlinear deflection and stress analysis of skew sandwich shell panel using higher-order theory, Eng. Comput. 35 (2) (2018) 467–485, https://doi.org/10.1007/s00366-018-0609-3.
[67] M. Rezaiee-Pajand, E. Arabi, A.R. Masoodi, Nonlinear analysis of FG-sandwich plates and shells, Aerosp. Sci. Technol. 87 (2019) 178–189, https://doi.org/10.1016/j.ast.2019.02.017.
[68] S. Serdoun, S.H. Cherif, Free vibration analysis of composite and sandwich plates by alternative hierarchical finite element method based on reddy's c1 HSDT, J. Sandw. Struct. Mater. 18 (4) (2016) 501–528, https://doi.org/10.1177/1099636215603033.
[69] J.N. Reddy, Mechanics of Laminated Composite Plates and Shells, CRC Press, 2004.
[70] O. Zienkiewicz, J. Zhu, Superconvergence and the superconvergent patch recovery, Finite Elem. Anal. Des. 19 (1–2) (1995) 11–23, https://doi.org/10.1016/0168-874x(94)00054-j.
[71] J. Akin, Super-convergent patch recovery, in: Finite Element Analysis with Error Estimators, Elsevier, 2005, pp. 146–177.
[72] F. Tornabene, N. Francesco, E. Viola, Inter-laminar stress recovery procedure for doubly-curved, singly-curved, revolution shells with variable radii of curvature and plates using generalized higher-order theories and the local GDQ method, Mech. Adv. Mat. Struct. 23 (9) (2016) 1019–1045, https://doi.org/10.1080/15376494.2015.1121521.
[73] F. Tornabene, N. Fantuzzi, M. Bacciocchi, J. Reddy, A posteriori stress and strain recovery procedure for the static analysis of laminated shells resting on nonlinear elastic foundation, Composites, Part B, Eng. 126 (2017) 162–191, https://doi.org/10.1016/j.compositesb.2017.06.012.
[74] F. Auricchio, E. Sacco, A mixed-enhanced finite-element for the analysis of laminated composite plates, Int. J. Numer. Methods Eng. 44 (10) (1999) 1481–1504, https://doi.org/10.1002/(SICI)1097-0207(19990410)44:10<1481::AID-NME554>3.0.CO;2.
[75] P.M. Daniel, J. Främby, M. Fagerström, P. Maimí, Complete transverse stress recovery model for linear shell elements in arbitrarily curved laminates, Compos. Struct. 252 (2020) 112675, https://doi.org/10.1016/j.compstruct.2020.112675.
[76] M. Ganapathi, B. Patel, D. Makhecha, Nonlinear dynamic analysis of thick composite/sandwich laminates using an accurate higher-order theory, Composites, Part B, Eng. 35 (4) (2004) 345–355, https://doi.org/10.1016/s1359-8368(02)00075-6.
[77] A.M. Zenkour, Three-dimensional elasticity solution for uniformly loaded cross-ply laminates and sandwich plates, J. Sandw. Struct. Mater. 9 (3) (2007) 213–238, https://doi.org/10.1177/1099636207065675.
[78] S. Levy, Square plate with clamped edges under normal pressure producing large deflections, 1942.
[79] T. Kant, J. Kommineni, C0 finite element geometrically non-linear analysis of fibre reinforced composite and sandwich laminates based on a higher-order theory, Comput. Struct. 45 (3) (1992) 511–520, https://doi.org/10.1016/0045-7949(92)90436-4.
[80] H. Nguyen-Van, N. Nguyen-Hoai, T. Chau-Dinh, T. Nguyen-Thoi, Geometrically nonlinear analysis of composite plates and shells via a quadrilateral element with good coarse-mesh accuracy, Compos. Struct. 112 (2014) 327–338, https://doi.org/10.1016/j.compstruct.2014.02.024.
[81] K.J. Bathe, E.N. Dvorkin, A four-node plate bending element based on Mindlin/Reissner plate theory and a mixed interpolation, Int. J. Numer. Methods Eng. 21 (2) (1985) 367–383, https://doi.org/10.1002/nme.1620210213.